Flows, scaling, and the control of moment hierarchies for stochastic chemical reaction networks

Eric Smith
Earth-Life Science Institute, Tokyo Institute of Technology, 2-12-1-IE-1 Ookayama, Meguro-ku, Tokyo 152-8550, Japan;
Department of Biology, Georgia Institute of Technology, 310 Ferst Drive NW, Atlanta, Georgia 30332, USA;
Santa Fe Institute, 1399 Hyde Park Road, Santa Fe, New Mexico 87501, USA;
and Ronin Institute, 127 Haddon Place, Montclair, New Jersey 07043, USA

Supriya Krishnamurthy
Department of Physics, Stockholm University, 106 91 Stockholm, Sweden
(Received 24 July 2017; published 1 December 2017)

Stochastic chemical reaction networks (CRNs) are complex systems that combine the features of concurrent transformation of multiple variables in each elementary reaction event and nonlinear relations between states and their rates of change. Most general results concerning CRNs are limited to restricted cases where a topological characteristic known as deficiency takes a value 0 or 1, implying uniqueness and positivity of steady states and surprising, low-information forms for their associated probability distributions. Here we derive equations of motion for fluctuation moments at all orders for stochastic CRNs at general deficiency. We show, for the standard base case of proportional sampling without replacement (which underlies the mass-action rate law), that the generator of the stochastic process acts on the hierarchy of factorial moments with a finite representation. Whereas simulation of high-order moments for many-particle systems is costly, this representation reduces the solution of moment hierarchies to a complexity comparable to solving a heat equation. At steady states, moment hierarchies for finite CRNs interpolate between low-order and high-order scaling regimes, which may be approximated separately by distributions similar to those for deficiency-zero networks and connected through matched asymptotic expansions. In CRNs with multiple stable or metastable steady states, boundedness of high-order moments provides the starting condition for recursive solution downward to low-order moments, reversing the order usually used to solve moment hierarchies. A basis for a subset of network flows defined by having the same mean-regressing property as the flows in deficiency-zero networks gives the leading contribution to low-order moments in CRNs at general deficiency, in a $1/n$ expansion in large particle numbers. Our results give a physical picture of the different informational roles of mean-regressing and non-mean-regressing flows and clarify the dynamical meaning of deficiency not only for first-moment conditions but for all orders in fluctuations.

DOI: 10.1103/PhysRevE.96.062102

I. INTRODUCTION

Random walks of multiple independent particles on ordinary graphs are simple processes in several fundamental senses [1–3]. Each step involves a change of a single degree of freedom, and for the base case of proportional sampling without replacement, the rate law for fluxes is linear in concentrations. Moreover, identification of topological properties of ordinary graphs that determine characteristics of random-walk dynamics can generally be carried out in polynomial time [1,4].

Just the opposite is true of the stochastic processes associated with chemical reaction networks (CRNs). Each elementary reaction event (for a general network) can involve the concurrent conversion of multiple inputs into multiple outputs [5,6], making the elementary network on which the reactions occur not an ordinary graph, but a directed multihypergraph [7,8]. For the base case of proportional sampling without replacement over reactants, the rate law becomes nonlinear, leading generically to possibilities for complex dynamics and multiple (stable or metastable) steady states [9–11]. Moreover, identification of key topological properties such as shortest reaction sequences connecting inputs to outputs or complete sets of self-amplifying cycles, which affect the character of CRN dynamics, are known to be NP-hard problems for hypergraphs [12,13].

As a consequence, although stochastic processes with the essential features of CRNs are ubiquitous in biochemistry [14], systems biology [15], ecology [16], and epidemiology [17] and are thus of large practical and theoretical interest, few results exist for these systems [18–22] compared with the large amount of literature that exists for random walks on ordinary graphs [1]. In addition to systems that clearly have CRN structure because the underlying processes obey constraints of stoichiometry (the source of concurrency), the CRN framework is flexible enough to furnish a representation for systems of broad interest to nonequilibrium thermodynamics such as the zero-range process [23], where topological characteristics that are known to lead to simple steady states for CRNs can be used to sieve for exactly solvable cases. Indeed, some of the key results that are known for stochastic CRNs [24] were motivated in part by earlier work of Kelly on a related class of queuing networks [25].

A. Partitioning off the simple subarchitecture in the core of complex CRNs

A representation scheme for CRNs was made standard by the work of Feinberg [9,18], which separates the structure of independent reaction events from the stoichiometric relations that determine their action in the chemical state space. We

will emphasize that, well beyond the use made by its original authors, this decomposition defines the fundamental partition in CRN architecture between a subsystem with the same simplicity as the random walk on an ordinary graph and the remainder of the CRN constraints responsible for concurrency, nonlinearity, and their resulting complexity. Identifying the subsystem isomorphic to a simple process is the key to decomposing the scaling behaviors in the moment hierarchies of CRNs and to distinguishing the roles of different classes of flows in the dynamics and steady states.

The emphasis in the work of Feinberg, and in closely related work by Horn and Jackson [26], was the existence and uniqueness of solutions to the mass-action rate equations with strictly positive concentrations: a limited, deterministic, and static problem. We will show below that the Feinberg decomposition is even more useful in the analysis of the stochastic processes associated with CRNs, where in addition to exact results in deterministic limits, it can serve as a foundation for systematic approximation methods in the general case. A host of results follow, including representations of the generator of the stochastic process acting on the moment hierarchy, duality relations of the kind explored in stochastic thermodynamics [27], and scaling relations that suggest solution methods using matched asymptotic expansions.

B. Expanded role for deficiency

A dimensional property termed deficiency was introduced by Feinberg [9], which was central both to the results on existence and uniqueness of steady states and to a limited but important corollary about the form of some of the distributions associated with such states. Deficiency can be computed as a topological index from the graphical structure associated with a CRN [9–11], but its importance comes from its meaning as a count of the dimensionality of chemical flows that can proceed in a steady state without being subject to mean regression due to changes in chemical concentrations. When there are no such regression-free flows, when deficiency equals zero, the network is guaranteed to have unique strictly positive steady states at general parameters. A remarkable result due to Anderson *et al.* [24] is that under the same conditions, the steady-state distributions have a simple factorial form under proportional sampling rules and a class of related forms under more general rules (e.g., Michaelis kinetics), as long as they sample chemical species independently of one another.

The concept expressed by deficiency remains key to organizing the stochastic processes for general CRNs, even when their deficiency is nonzero, and the clues for why this should be so are already latent in the Anderson-Craciun-Kurtz (ACK) theorem [24]. For the simple case of proportional sampling without replacement (which gives rise to mass-action kinetics and which we will assume in the remainder of the article), the ACK solutions are either products of Poisson distributions or hypersurfaces within such product-Poisson distributions constrained by particle conservation laws (with no loss of generality for the claims below). In a Poisson distribution, all higher moments are universal functions of the mean value, so in a product of Poisson distributions, the entire moment hierarchy is controlled by the set of first moments. In a deficiency-zero network at steady state, the ACK theorem effectively states that first-moment values carry all the "information" in the distribution. When deficiency is nonzero, the mean-regressing flows are no longer the exclusive dynamical entities, but as we will show they remain the dominant entities governing low-order moments, in an asymptotic expansion where the small parameter is the order of any moment of the distribution relative to its mean particle number. The approach by which we will construct this result also shows how to extract other scaling regimes associated with the remaining flows in networks with nonzero deficiency and the way these control complementary asymptotic expansions for high-order moments relative to mean particle numbers.

C. Coupling CRN theory to Doi operator algebras for stochastic processes

Our approach to the stochastic processes associated with CRNs grows out of a set of linear-algebra methods due to Doi [28,29], for the treatment of generating functions for general discrete-state stochastic processes. The Doi operator algebra provides a starting point for numerous solution methods,[1] but its simplifying effect is particularly elucidating for CRNs. In the classical mass-action theorems of Feinberg, the rate equations for CRNs take an awkward and not-very-perspicuous form, in which stoichiometry is expressed asymmetrically in nonlinear rate laws and concurrency constraints on inputs and outputs. In the Doi representation of the full stochastic process, all formal asymmetry between inputs and outputs disappears. It can be seen that the asymmetry of the Feinberg problem reflects the way the particular projection operator to the first-moment equations of motion interacts with the formally symmetric generator of all fluctuations. Within the framework of the Doi algebra, we formulate the projection operator that gives the equations of motion for arbitrary moments and show how the Feinberg equations generalize to a representation of the generator of the stochastic process acting on the moment hierarchy, which directly expresses the scaling influence of different network flows. The underlying symmetry of the Doi representation of the stochastic process generator remains and can serve as a point of departure for the derivation of duality relations for stochastic CRNs, which we mention here but develop elsewhere [32]. Some of our results emphasizing the simplification of stochastic CRN analysis in the Doi formalism have been derived earlier in [33], particularly the proof of the ACK theorem in our Sec. IV B.

D. Organization of the presentation

The presentation is organized as follows.

In Sec. II we introduce the general concepts and notation associated first with chemical reaction networks, then with general discrete-state stochastic processes, and finally for the particular forms of stochastic processes associated with CRNs. The culmination of this section is Eq. (27), the Liouville-form

[1]One of the best known of these is the coherent-state expansion of generating functionals due to Peliti [30,31]. It is particularly useful for semiclassical approximations and other stationary-point methods, which we mention but do not pursue in depth here.

expression for the generator of the stochastic process of a CRN motivated by the Feinberg decomposition, which is the basis for all other results in the paper.

Section III introduces the factorial moments that are the natural observables for CRNs with simple mass-action rate laws and shows that a dynamical equation for all orders of fluctuations is closed and has a finite-order generator in this set of moments. The culmination of this section is the representation of the generator in Eq. (34).

Section IV then shows how topological characteristics of the CRN are linked to dynamical properties of flows and reviews the Feinberg deficiency-zero theorem and the associated Anderson-Craciun-Kurtz theorem. We introduce what we term the stoichiometric decomposition of the Liouville operator in Eq. (40), which separates two dynamically different classes of mean-regressing and non-mean-regressing flows.

Section V uses the representation of the generator on the lattice of factorial moments to show how different combinations of rate constants from a CRN govern scaling properties of moments in different ranges of the moment order. This section shows how matched asymptotic expansions can be used to solve for steady-state moment hierarchies recursively and shows the (related) sense in which the deficiency-zero-like subset of flows in the stoichiometric decomposition dominates low-order moments. Section VI then provides a sequence of worked examples of ascending complexity to introduce each of the concepts above and show its effects in a solution.

We have chosen to develop all main results in their general forms in Secs. II–V, in the interest of economy and continuity of the argument, postponing examples to Sec. VI, where they may be directly compared. The simplest case and the starting point involves one species and deficiency zero (Sec. VI A), illustrating the way the ACK theorem is recovered in the Doi algebra with a one-line proof. We then introduce nonzero deficiency while keeping the same mass-action equations of motion (Sec. VI B), to show how the subspace of flows resembling a zero-deficiency network can be extracted (but also why, in the general case, this cannot be expressed as a zero-deficiency subprocess of the full process) and how it controls the scaling of low-order moments. Next we hold the deficiency fixed but change the network topology to one in which autocatalytic feedback produces multiple steady states in the mass-action approximation (Sec. VI C). This case introduces the first nontrivial role for the asymptotic expansion and shows, counterintuitively, how a criterion of boundedness for asymptotically high-order moments anchors the recursion downward to specify the low-order moments of the ergodic distribution over the two steady states. All effects up to this point are illustrated with single-species networks. At the end we introduce a two-species network in which cross catalysis replaces the single-species autocatalysis (Sec. VI D), yielding an equivalent bistable classical system if the species are not distinguished. This case demonstrates a nontrivial use of the stochastic process generator acting on the moment hierarchy and shows how the factorability of the ACK theorem for multispecies distributions is lost at nonzero deficiency.

Readers who prefer to alternate general notation and instances are encouraged to browse the examples in Sec. VI in parallel with reading the formal development in the earlier sections. A more direct track to the main results on recursions in the moment hierarchy is also provided in [34].

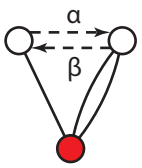

FIG. 1. Graphical representation for a minimal CRN model and the first example in the sequence that will be developed in Sec. VI: one chemical species, two complexes, a single linkage class, and deficiency zero. These terms are defined in the remainder of the section.

II. CHEMICAL REACTION NETWORKS AND THEIR ASSOCIATED STOCHASTIC PROCESSES

The next three sections review the standard concepts for CRNs and two aspects of stochastic-process algebras (representations of the generator and then the Doi operator formalism) and introduce the notation in which we will represent them in this paper. In Sec. II D these are then brought together to obtain the Liouville-operator representation of the generator for a stochastic process CRN that will be the basis for all further constructions.

A. Elements of a CRN

Our decomposition of CRNs follows that of Feinberg [9], but we use a more complete graphic representation, illustrated for our simplest example process in Fig. 1. We will present CRNs using both this graphic form and a corresponding reaction-scheme form such as

$$A \underset{\beta}{\overset{\alpha}{\rightleftharpoons}} 2A. \tag{1}$$

The following list explains the fundamental division of Feinberg and of Horn and Jackson that separates the so-called complex network[2] from the stoichiometric relations that interpret its action in the state space of chemical species.

The chemical species. In examples we will denote explicit species names by single capital roman letters such as A. Where a set of species is indicated, we index them with subscripts $p \in 1, \ldots, P$, the number of distinct chemical species. In network diagrams a species is denoted with a filled dot: ●

Complex: a multiset of species, which is the input or output of a reaction. It may be written as a sum rather than a set. Examples might be A or $2A$ (or equivalently $A + A$). In network diagrams, a complex is denoted by an open circle with one or more (labeled) dashed line stubs indicating the reaction(s) in which it participates and (labeled) solid line stubs indicating the participating species: ⋑○--- (In one-species or one-reaction networks, or after the network diagram has been assembled, we may suppress the labels to improve readability.) In set notation, we index complexes with subscripts i or j.

[2]Here the stress is on the first syllable, 'com,plex network, to be distinguished from references to systems that are com'plex.

(Directed) reaction: An ordered pair of complexes with an associated rate constant. For complexes indexed i and j, respectively, the reaction from i to j would correspond to the ordered pair (i, j) and the associated rate constant is denoted by k_{ji}. (For simple models, rate constants may be given simplifying labels such as α.)

An expression with one or more reaction is known as a reaction scheme, such as

$$A \overset{\alpha}{\rightharpoonup} 2A. \tag{2}$$

In network diagrams, a reaction is represented with a dashed arrow between the input and output complexes (optionally labeled with the rate constant): $\text{--}\overset{\alpha}{\text{-}}\!\!\rightarrow$

Chemical Reaction Network (CRN): a collection of reactions. By default we adopt the finest-grained description in which all reactions are unidirectional; bidirectional reactions are indicated with pairs of directed arrows. In reaction schemata we may also condense notation for bidirectional reactions, as above in scheme (1).

Graphically, a CRN is a well-formed doubly bipartite network (two kinds of nodes and two kinds of links), in which all reactions terminate in two complexes, and all line stubs from a complex are filled by the appropriate reactions or links to chemical species,[3] as in Fig. 1.

Adjacency-rate matrix. In Feinberg's representation of CRNs [9,18], only the complexes and the reactions are denoted explicitly and they form an ordinary directed graph. In a stochastic formulation, reactions can occur as independent events on the links, analogous to the steps in a simple random walk. Complexes are treated as if they have activities and the set of rate constants map these activities to reaction rates. In this way, both stoichiometric constraints and the determination of activities of complexes are cordoned off as separate information from the rate and connectivity structure of the complex network. The latter is given by an ordinary adjacency-rate matrix, identical in form to the graph Laplacian for a simple random walk. Following the notation made standard by Feinberg, we denote this matrix by $\mathbb{A}$.

Arranging complexes in a column vector indexed by i, let w_i be the indicator function that is nonzero on complex i only [so the jth component $(w_i)_j \equiv \delta_{ij}$] and w_i^{T} its transpose, which can act as a projection operator. Then the adjacency-rate matrix can be written as a sum of dyadics, arranged in a variety of ways. Two of these we call the reaction representation and the complex representation, written, respectively,

$$\begin{aligned}\mathbb{A} &= \sum_{(i,j)} (w_j - w_i) k_{ji} w_i^{\mathsf{T}}, \\ &= \sum_i w_i \sum_j \left(k_{ji} w_j^{\mathsf{T}} - k_{ij} w_i^{\mathsf{T}}\right).\end{aligned} \tag{3}$$

In expressions such as the canonical mass-action rate law, which will appear as Eq. (41) below, after its context has been properly introduced, the row vectors w^{T} select the activities determining reaction rates and the column vectors w identify the net flux into and out of complexes. The reaction representation is often more intuitive for constructing generators of the stochastic process, while the complex representation, in accumulating all flows into or out of a complex, more directly reflects the cause of mean regression that underlies the concept of deficiency.

Stoichiometric matrix. In order to connect complexes to species, let N, representing a state of the reactor, denote the column vector $N \equiv [N_p]$ in which element N_p is the count of species p, and introduce a matrix Y with rows $y_p \equiv [y_p^i]^{\mathsf{T}}$, where y_p^i are the stoichiometric coefficients indicating the number of instances of species p in complex i. In graphs such as Fig. 1, this is the number of solid lines from the species node p to the complex node i. The product $Y\mathbb{A}$ connects fluxes at complexes (the row index on $\mathbb{A}$) to fluxes at species (the row index on $Y\mathbb{A}$).

Interpretation of complex activities. Complexes are not the same as chemical species and their (virtual) activities in the Feinberg complex graph must be fixed in terms of the (actual) activities of the species. We will call any such dependence an interpretation of the complexes.[4]

To give an interpretation of complex activities in terms of species activities that is convenient to use with the adjacency-rate matrix, let $\Psi_Y \equiv [\Psi_Y^i]$ be a column vector with components given by

$$\Psi_Y^i(N) \equiv \prod_p \frac{N_p!}{(N_p - y_p^i)!}. \tag{4}$$

Here Ψ_Y defines the activity products corresponding to proportional sampling without replacement on the discrete indices N_p. We will return below to the relation between discrete sampling and mass-action rate laws, after we have introduced notation and concepts for the stochastic process that governs mass action and all higher moments.

B. Representations of a stochastic process

A certain standard machinery underlies all discrete-state stochastic processes, including those associated with CRNs. Before deriving the particular forms for the network decomposition of Sec. II A, we introduce general notation and constructions in this section.

The point we wish to emphasize is that, while the stochastic process for a CRN has a uniquely defined generator, that

[3]Strictly speaking, a CRN corresponds to a directed multihypergraph, in which the reactions correspond to directed hyperedges and the input and output complexes are their vertex sets. The graphic depiction used here and elsewhere is a bipartite representation of the underlying hypergraph. The computational complexity of numerous search and optimization problems on hypergraphs, which are simple on ordinary graphs, is one consequence of the concurrency of inputs and outputs on a hyperedge.

[4]It is an interesting question, which we leave for other work, whether the random walk on the complex network can be represented formally in terms of a linear algebra of pseudoparticles, which are formal proxies for the products of operators representing real particles of the chemical species.

generator may have many representations, depending on whether we solve the stochastic process for its probability density, the moment-generating function of that density, or the hierarchy of moments evaluated directly. When the activities of complexes are defined by proportional sampling without replacement as in Eq. (4) (the simplest case, corresponding to ideal gases or solutions), the moments that appear naturally in all rate equations are what we term factorial moments, and it is for these that the equations of motion take the most compact form.

The essential components in the stochastic-process description are then the following.

Probability density function and transfer matrix. States of the CRN are indexed by values of the vector N and reactions are treated as instantaneous changes of state.[5] Our starting point in describing the stochastic process is a probability density function ρ_N indexed on the values of N.

The density ρ evolves on a time coordinate τ under a master equation

$$\frac{\partial \rho}{\partial \tau} = T\rho,$$

which is shorthand for

$$\frac{\partial \rho_N}{\partial \tau} = \sum_{N'} T_{NN'}\rho_{N'}. \tag{5}$$

The matrix $T \equiv [T_{NN'}]$ is called the transfer matrix and is one representation of the generator of the stochastic process.

Moment-generating function and Liouville operator. The moment-generating function is formed from ρ_N with the introduction of a vector $z \equiv [z_p]$ of complex coefficients, as the Laplace transform

$$\phi(z) \equiv \sum_N \left(\prod_p z_p^{N_p}\right)\rho_N. \tag{6}$$

The generating function evolves under a Liouville equation of the form

$$\frac{\partial \phi}{\partial \tau} = -\mathcal{L}\phi,$$

which is shorthand for

$$\frac{\partial}{\partial \tau}\phi(z) = -\mathcal{L}\left(z, \frac{\partial}{\partial z}\right)\phi(z). \tag{7}$$

Here $\mathcal{L}$ is called the Liouville operator. Its form is defined from the transfer matrix in Eq. (5) and it provides an alternative representation of the generator of the stochastic process, acting on Laplace transforms.

Expectations and moments and their time dependence. The expectation of an arbitrary function $\mathcal{O}(N)$ (for observable) of the components of N, in the background ρ, will be denoted with angle brackets, as

$$\langle \mathcal{O}(N)\rangle \equiv \sum_N \mathcal{O}(N)\rho_N. \tag{8}$$

Since ρ may be a continuous-valued quantity whereas N is discrete, we introduce a particular shorthand with math-italic font for the first moment

$$n \equiv \langle N\rangle = \sum_N N\rho_N, \tag{9}$$

which may vary continuously if ρ does. The mass-action rate equations are expressed entirely in terms of n. Depending on the form of the underlying distribution ρ and whether higher-order correlations can be expressed as functions of n, the mass-action equations may be exact or they may involve a (generally unregulated) approximation known as the mean-field approximation.

The first moment n may also be obtained from the generating function as

$$n = \frac{\partial}{\partial z}\ln\phi(z)\bigg|_{z\equiv 1} \tag{10}$$

and expectations of more complex observables can be built up by acting on ϕ appropriately with higher-order derivatives in z. The time dependence of n, which is the object of classical first-moment equations or chemical rate equations, can be obtained by acting on either ρ or ϕ with its corresponding generator, by Eq. (5) or (7).

Factorial moments for CRNs. In many applications, the natural moments for which to study dynamics are either ordinary powers N^k, obtained by acting on ϕ with higher derivatives in z, or cumulants [35], obtained by acting on $\ln\phi$ with higher derivatives in z. For CRNs with reaction rate laws corresponding to proportional sampling without replacement, however, the simplest dynamical relations are obtained for the factorial moments, for which we therefore introduce specific notation. For a single component N_p and power k_p,

$$N_p^{\underline{k_p}} \equiv \begin{cases} \frac{N_p!}{(N_p-k_p)!}, & k_p \leqslant N_p \\ 0, & k_p > N_p. \end{cases} \tag{11}$$

[We adopt the convention in the second line of Eq. (11) for $k_p > N_p$ because it allows a simplification in sum notations below.] We will use the form of Eq. (11) as a general formula for truncated factorials,[6] allowing other integer-valued arguments such as stoichiometric coefficients to take the place of N_p as the argument.

Moment hierarchy and another representation for the generator. For a vector $k \equiv [k_p]$ of powers, we introduce the factorial moment hierarchy indexed by k, as the expectation

$$\Phi_k \equiv \left\langle \prod_p N_p^{\underline{k_p}} \right\rangle. \tag{12}$$

We show in Sec. III that Φ evolves in time as

$$\frac{\partial \Phi}{\partial \tau} = \Lambda\Phi,$$

[5]This level of coarse graining in the description of reaction events is the standard assumption also in stochastic thermodynamics [27].

[6]These truncated factorials are known in the mathematics literature as falling factorials or falling powers [33].

which is shorthand for

$$\frac{\partial \Phi_k}{\partial \tau} = \sum_{k'} \Lambda_{kk'} \Phi_{k'}. \tag{13}$$

The matrix $\Lambda \equiv [\Lambda_{kk'}]$ has finitely many nonzero entries determined by the stoichiometric coefficients and its form may be derived from the Liouville operator $\mathcal{L}$. The matrix Λ provides yet a third representation of the generator of the stochastic process, which is particularly well suited to the study of CRNs because it exposes different scaling regimes controlled by combinations of the rate parameters corresponding to different flows. We develop the implications of scaling in Sec. V.

C. Doi operator algebra for a discrete-state stochastic process

For most of its purposes as a generating function, it is not necessary that $\phi(z)$ be an analytic function of a vector z of complex-valued arguments. Often only the formal power series in z, together with its algebra with the derivative $\partial/\partial z$, is required.

The abstraction of the linear algebra of generating functions in terms of formal raising and lowering operators follows a procedure due to Doi [28,29]. We have elaborated the details of the mapping and its interpretation extensively elsewhere [36–38], so here we only summarize the notation, which by now is standard.[7]

The Doi algebra denotes the argument variables and their derivatives as abstract raising and lowering operators,

$$z_p \to a_p^\dagger, \quad \frac{\partial}{\partial z_p} \to a_p, \tag{14}$$

because partial differentiation then imposes on these operators the conventional commutation algebra

$$[a_p, a_q^\dagger] = \delta_{pq}, \tag{15}$$

where δ_{pq} is the Kronecker δ. Generating functions, which are polynomials multiplying the number 1, are written as the action of the raising operators on a formal right-hand null state, while the projection operator that takes the trace of a generating function with an integral is written as a left-hand null state

$$1 \to |0), \quad \int d^P z\, \delta^P(z) \to (0|, \tag{16}$$

where $\delta^P(z)$ is the Dirac δ in P dimensions and the inner product of the null states is normalized: $(0|0) = 1$.

[7]Indeed, most treatments open directly with the Doi algebra [39,40]. We have used the two-step introduction by way of conventional analytic generating functions because it clarifies the meaning of some terms in the Doi algebra that can be obscure when presented without introduction. Reference [33] is the only other introduction we have seen that makes the same choice and the presentation is closely parallel.

The basis for generating functions is the set of number states that are elementary monomials. For any vector N,

$$\prod_{p=1}^{P} z_p^{N_p} \times 1 \to \prod_{p=1}^{P} a_p^{\dagger\, N_p} |0) \equiv |N); \tag{17}$$

number states are eigenstates of the set of number operators $a_p^\dagger a_p$:

$$a_p^\dagger a_p |N) = N_p |N). \tag{18}$$

In particular, for use with CRNs, we note the role of lowering operators in extracting the truncated factorials of number arguments: For any non-negative integer k,

$$a_p^k |N) = N_p^{\underline{k}} |N - k_p), \quad a_p^{\dagger\, k} a_p^k |N) = N_p^{\underline{k}} |N), \tag{19}$$

where $|N - k_p)$ is the number state with k subtracted from N_p and all N_q for $q \neq p$ unchanged.

With these steps the generating function becomes a vector in a linear space:

$$\phi(z) = \sum_N \prod_{p=1}^{P} z_p^{N_p} \rho_N \to \sum_N \rho_N |N) \equiv |\phi). \tag{20}$$

All number states are normalized with respect to the Glauber inner product, defined by

$$(0| \exp\left(\sum_p a_p\right) |N) = 1, \quad \forall N, \tag{21}$$

and the Glauber inner product with a generating function is simply the trace of the underlying probability density

$$(0| \exp\left(\sum_p a_p\right) |\phi) = \sum_N \rho_N = 1. \tag{22}$$

The above conventions define the standard representation in which we will work with generating functions in the remainder of this article.

D. Stochastic process for a CRN

We now apply the above operator formalism to the particular forms of transfer matrices and generating functions produced by CRNs and show how the reaction and complex representations decompose the resulting representations of the generators. Corresponding to the column vector Ψ_Y of activities from Eq. (4), we introduce a second column vector $\psi_Y \equiv [\psi_Y^i]$ that takes as its argument the Doi lowering operators a_p that extract the truncated factorials of N_p according to Eq. (19). Making use of the notation (11) for these truncated factorials, we may write the coefficients in these two vectors as

$$\Psi_Y^i(N) \equiv \prod_p N_p^{\underline{y_p^i}}, \quad \psi_Y^i(a) \equiv \prod_p a_p^{y_p^i}. \tag{23}$$

There is a corresponding row vector for the adjoints: $\psi_Y^\dagger \equiv [\psi^{\dagger\, i}_Y]^{\mathsf{T}}$ is a row vector of components defined on the complex

indices i, where the notation means

$$\psi^{\dagger i}_{Y}(a^{\dagger}) \equiv \prod_{p} a^{\dagger y^{i}_{p}}_{p}. \tag{24}$$

[As we did with the notation (11) for factorial moments, we take the definitions (23) and (24) for ψ and $\psi^{\dagger}$ as general forms, in which other arguments besides a and $a^{\dagger}$, such as the first-moment value n, can appear. This is convenient when expressing the approximation made in the mass-action rate law and exhibiting its relation to the exact equation of motion as an operator expression.]

We now use the above notation to group the sample numbers and index shifts that describe the concurrent conversion of reactants into products in the elementary reaction events of a CRN. We begin with the transfer matrix and then show the simplifications afforded by working with the Liouville operator.

For proportional sampling without replacement, the number dependence of the probability for the reaction (i, j) from state N is simply given by the component $\Psi^{i}_{Y}(N)$ from Eq. (23). The way the master equation acts on indices is slightly more complicated: For the delivery of probability into state N, the master equation must sample both ρ and Ψ^{i}_{Y} at a value shifted from N by the stoichiometric coefficients that are consumed at complex i minus those that are produced at complex j. The simplest way to express such shifts is to let the vector of shift operators $e^{\partial/\partial N}$ (with the exponential evaluated componentwise on N) serve as an argument to ψ^{i}_{Y}, thus

$$\psi^{i}_{Y}(e^{\partial/\partial N}) \equiv \prod_{p} e^{y^{i}_{p}\partial/\partial N_{p}} = e^{y^{i\mathsf{T}}\partial/\partial N}; \tag{25}$$

with this convention for both the rate constant and the shift operator, the matrix T from Eq. (5) can be written

$$\begin{aligned} T &= \psi^{\dagger}_{Y}(e^{-\partial/\partial n})\mathbb{A}[\psi_{Y}(e^{\partial/\partial n}) \cdot \Psi_{Y}(N)] \\ &= \sum_{(i,j)} \left[\psi^{j}_{Y}(e^{-\partial/\partial n}) - \psi^{i}_{Y}(e^{-\partial/\partial n})\right] k_{ji} \psi^{i}_{Y}(e^{\partial/\partial n}) \Psi^{i}_{Y}(N). \end{aligned} \tag{26}$$

Here the dot product between $\psi_{Y}(e^{\partial/\partial n})$ and $\Psi_{Y}(N)$ in the first line indicates that these two vectors are to be multiplied componentwise with respect to the complex index i so that their product is then extracted by the indicator functions w^{T}_{i} in $\mathbb{A}$ from Eq. (3). The cross term in ψ^{j}_{Y} and $\psi^{i}_{Y}\Psi^{i}_{Y}$, made explicit in the second line of Eq. (26), performs the required index shift on N in both ρ and Ψ_{Y} to account for the particles lost from the system's state through complex i and those gained by the system's state through complex j. The other cross term, with $\psi^{i}_{Y}(e^{-\partial/\partial n})$, simply cancels the shift operators in $\psi^{i}_{Y}(e^{\partial/\partial n})$ and represents the loss of probability from state N with rate $\Psi^{i}_{Y}(N)$.

Working with the Liouville operator from Eq. (7) is much more straightforward, because the lowering operators a_{p} both extract sample numbers and shift indices according to Eq. (19), so these do not need to be separately tracked as they are in the transfer matrix. Using the exact definitions (23) and (24) with the arguments a and $a^{\dagger}$ implicit, $\mathcal{L}$ takes the form

$$-\mathcal{L} = \psi^{\dagger}_{Y}\mathbb{A}\psi_{Y}. \tag{27}$$

Equation (27) is one of the central equations of this paper and underlies many of the simplifications we present here. In this expression, all the formal asymmetry of the standard first-moment rate equations from the CRN literature has disappeared and particle consumption and creation are now treated symmetrically. This is the first of many simplifications gained by working with the Laplace transform and the Doi operator algebra.

III. DYNAMICS OF MOMENT HIERARCHIES

From the foregoing constructions we can directly compute the equations of motion for arbitrary moments of the density ρ_{N}. These equations are finitely generated if we work in a basis of factorial moments, the demonstration of which is the main result of this section.

A. Dynamics of factorial moments for a single species

For a non-negative integer k, the operator that extracts the truncated factorial $N^{\underline{k}}_{p}$ from number states, which are the basis for a general state vector $|\phi)$, is a^{k}_{p}. Therefore, the expectation of $N^{\underline{k}}_{p}$ in the state $|\phi)$ is given by

$$\langle N^{\underline{k}}_{p}\rangle = (0|\exp\left(\sum_{q} a_{q}\right) a^{k}_{p}|\phi), \tag{28}$$

and from Eq. (7) and the form (27) for $\mathcal{L}$, its time dependence is given by

$$\begin{aligned} \frac{\partial}{\partial\tau}\langle N^{\underline{k}}_{p}\rangle &= (0|\exp\left(\sum_{q} a_{q}\right) a^{k}_{p}(-\mathcal{L})|\phi) \\ &= (0|\exp\left(\sum_{q} a_{q}\right) a^{k}_{p}\psi^{\dagger}_{Y}(a^{\dagger})\mathbb{A}\psi_{Y}(a)|\phi). \end{aligned} \tag{29}$$

In order to obtain a recursion relation for the time dependence of $\langle N^{\underline{k}}_{p}\rangle$ in terms of the values of other factorial moments, we must commute the product of lowering operators a^{k}_{p} through all powers of raising operators, which are gathered in the coefficients of the row vector $\psi^{\dagger}_{Y}$. The result of the commutation is a finite series with descending powers of a_{p} and $a^{\dagger}_{p}$. For positive integers k and y, the evaluation of operator products of powers of raising and lowering operators is given by[8]

$$\begin{aligned} a^{k}_{p}a^{\dagger y}_{p} &= \sum_{j=0}^{\min(k,y)} \frac{k!y!}{j!(k-j)!(y-j)!} a^{\dagger y-j}_{p} a^{k-j}_{p} \\ &= \sum_{j=0}^{k} \binom{k}{j} y^{\underline{j}} a^{\dagger y-j}_{p} a^{k-j}_{p}. \end{aligned} \tag{30}$$

The first line emphasizes the symmetric roles of k and y in the combinatorial coefficient. In the second line we have used the

[8]The proof is by induction. If $k \geqslant y$, start with an elementary evaluation of $a^{k}_{p}a^{\dagger}{}^{y}_{p}$ and then induct on y. If $k \leqslant y$, start with an elementary evaluation of $a_{p}a^{\dagger y}_{p}$ and induct on k.

definition (11) applied to $y^{\underline{j}}$ (rather than $N^{\underline{j}}$) to simplify the index of summation in the case that $k > y$.

Now we may expand the evaluation appearing in Eq. (29), using the sum (30),

$$\begin{aligned}
&(0|\exp\left(\sum_q a_q\right)a_p^k\psi^{\dagger i}_Y(a^\dagger)\\
&\quad=(0|\sum_{j=0}^{k}\binom{k}{j}(y_p^i)^{\underline{j}}\exp\left(\sum_q a_q\right)a_p^{k-j}\\
&\quad=\sum_{j=0}^{k}\binom{k}{j}(y_p^i)^{\underline{j}}(0|\exp\left(\sum_q a_q\right)a_p^{k-j},
\end{aligned}\tag{31}$$

as an operator identity acting on general states. Here we have used the property of the Doi operator algebra that commutation through the exponential $\exp(\sum_q a_q)$ shifts all $a_p^\dagger \to a_p^\dagger + 1$, after which all factors of $a_p^\dagger$ annihilate the right ground state $(0|$. Thus we have eliminated all factors of $a^\dagger$, along the way extracting from $\psi_Y^\dagger$ the factorial moments $(y_p^i)^{\underline{j}}$ of the stoichiometric coefficients.

The powers of the lowering operator a_p^{k-j} in Eq. (31) are the same form as terms already in ψ_Y, so we can absorb them into ψ_Y by shifting the stoichiometric coefficients in row p, which we denote as

$$\begin{aligned}
&(0|\exp\left(\sum_q a_q\right)a_p^{k-j}\psi_Y(a)|\phi)\\
&\quad=(0|\exp\left(\sum_q a_q\right)\psi_{Y+(k-j)_p}(a)|\phi)\\
&\quad=\left\langle\Psi_{Y+(k-j)_p}(N)\right\rangle.
\end{aligned}\tag{32}$$

Here $Y+(k-j)_p$ is the matrix in which the $\cdot_p^i$ component is $y_p^i + k - j \forall i$ and y_q^i is unchanged for $q \neq p$.

From these evaluations we can reexpress Eq. (29) as

$$\begin{aligned}
\frac{\partial}{\partial\tau}\langle N_p^{\underline{k}}\rangle &= \sum_{j=0}^{k}\binom{k}{j}Y_p^{\underline{j}}\mathbb{A}\left\langle\Psi_{Y+(k-j)_p}(N)\right\rangle\\
&= \sum_{j=1}^{k}\binom{k}{j}Y_p^{\underline{j}}\mathbb{A}\left\langle\Psi_{Y+(k-j)_p}(N)\right\rangle\\
&\equiv \sum_{j=1}^{k}\binom{k}{j}Y_p^{\underline{j}}e^{(k-j)\partial/\partial Y_p}\mathbb{A}\langle\Psi_Y(N)\rangle.
\end{aligned}\tag{33}$$

Here $Y_p^{\underline{j}}$ is a row vector in which the ith component is the factorial moment $(y_p^i)^{\underline{j}}$. Note that $Y_p^{\underline{0}}$ is the row vector of 1's, $Y_p^{\underline{1}} = Y_p$ the pth row of Y, etc. The first line of Eq. (33) contains the full sum over j from Eq. (31) and the second line uses the fact that $1^\mathsf{T}\mathbb{A} \equiv 0$ to eliminate the $j = 0$ term. In the third line, we have expressed the shift of coefficients in the pth row of Y again using an exponential shift operator denoted by $e^{\partial/\partial Y_p}$, which acts on all components y_p^i. This will be convenient notation for working with moments involving multiple species.

B. Generator of the stochastic process acting on the moment hierarchy

For multiple species, we generalize the notation to an integer-valued vector of powers $k \equiv [k_p]$ and arrange summation indices similarly in vectors $j \equiv [j_p]$. Recalling the definition (12) of the factorial moment hierarchy Φ, we write its time derivative as

$$\begin{aligned}
\frac{\partial}{\partial\tau}\Phi_k &\equiv \frac{\partial}{\partial\tau}\left\langle\prod_p N_p^{\underline{k_p}}\right\rangle\\
&= \dot{\prod_p}\left[\sum_{j_p=0}^{k_p}\binom{k_p}{j_p}Y_p^{\underline{j_p}}e^{(k-j)_p\partial/\partial Y_p}\right]\mathbb{A}\langle\Psi_Y(N)\rangle\\
&= \sum_{j_1=0}^{k_1}\binom{k_1}{j_1}\cdots\sum_{j_P=0}^{k_P}\binom{k_P}{j_P}\left[\dot{\prod_p}Y_p^{\underline{j_p}}\right]\mathbb{A}\langle\Psi_{Y+(k-j)}(N)\rangle\\
&\equiv \sum_{k'}\Lambda_{kk'}\Phi_{k'},
\end{aligned}\tag{34}$$

where the second line is an expansion of the first. The notation $\dot{\prod}_p$ denotes a product over species p within each index i of the row vectors $Y_p^{\underline{j_p}}$. (Note that in the sums over j_p, we must now retain the $j_p = 0$ entries, because even if one index $Y_p^{\underline{j_p}} = [1]^\mathsf{T}$, there may be others in the sum where $j_{p'} \neq 0$ and the product $(\dot{\prod}_p Y_p^{\underline{j_p}})\mathbb{A}$ is only ensured to vanish when all $j_p = 0$.) Now the shift operator $e^{(k-j)_p\partial/\partial Y_p}$ in the first line of Eq. (34) offsets all coefficients y_p^i in the row p by $(k-j)_p$, so we write the matrix Y in the second line with its rows shifted uniformly by the entries in the column vector $(k-j)$.

The third line of Eq. (34) gives the definition of the matrix Λ introduced in Eq. (13). Each entry in the matrix $\Psi_{Y+(k-j)}(N)$ is itself a truncated factorial, so the expression is closed on Φ. Although the orders k_p may be arbitrarily large, the matrix Λ has only finitely many nonzero entries, limited by the largest values of j_p for which the rows $Y_p^{\underline{j_p}}$ have nonvanishing entries [recalling the definition (11) for truncated factorials].

Equation (34) is the main result with which we will work in this paper. It contains the rate equations for the species numbers n studied by Feinberg and by Horn and Jackson and extends these to give a compact representation for the dynamics of all higher-order moments as well. In Sec. VI we illustrate graphic methods for representing Λ.

IV. NETWORK TOPOLOGY, DEFICIENCY, AND CLASSIFICATION AND ROLE OF DIFFERENT NETWORK FLOWS

The results up to this point are true for a general CRN. Thus they say nothing directly about the topological properties that may afford simplifications such as uniqueness and positivity of steady states or factorability of distributions. In this section we shift to a consideration of topology and its implications, including the concept of deficiency and the Feinberg [18] and Anderson-Craciun-Kurtz (ACK) theorems [24].

A. Deficiency and a basis to decompose network flows

The connectivity of the adjacency matrix $\mathbb{A}$, together with the stoichiometric matrix Y, determines the linear subspace of

N values that can be accessed through any flow on the network, called the stoichiometric subspace. Below, let ker(*) and im(*) denote the kernel and image, respectively, of the linear map which is their argument.

The number and character of steady states depend on whether the N dependence of the mass-action rate equations within this subspace admits a Lyapunov function [11,26]. That in turn depends on whether all flows that transport net matter into or out of any complex must also transport some net matter into or out of some chemical species, thus increasing its chemical potential in a direction that opposes the flow. If so, then all the flows are mean regressing and strictly positive steady states are unique. If not, there are net fluxes at the complexes that do not lead to net fluxes of species and for these there is no force leading to mean regression. In the latter case, multiple steady states or nonstrictly positive steady states[9] cannot be ruled out [19,20].

The character of the dynamical steady states therefore depends on the relative dimension of $\ker \mathbb{A}$ (the flows that absorb or emit no material at the complexes) and $\ker Y\mathbb{A}$ (the flows that absorb or emit no material at the chemical species), within the stoichiometric subspace. A sketch of the demonstration that this is a topological characteristic, following Feinberg [9,18] and Horn and Jackson [26], follows.

For any CRN, the stoichiometric subspace corresponds to

$$S \equiv \mathrm{im}(Y\mathbb{A}). \tag{35}$$

The dimensions of S and of the subspace of flows through complexes that do not produce motions within S are defined as

$$s \equiv \dim(S), \quad \delta \equiv \dim[\ker(Y) \cap \mathrm{im}(\mathbb{A})]. \tag{36}$$

Here δ is the deficiency of the CRN.

The following relations hold (as identities) among dimensions in $Y\mathbb{A}$ and $\mathbb{A}$:

$$\begin{aligned}\dim[\mathrm{im}(\mathbb{A})] &= \dim[\mathrm{im}(Y\mathbb{A})] + \dim[\ker Y \cap \mathrm{im}(\mathbb{A})] \\ &= s + \delta. \end{aligned} \tag{37}$$

If C is the total number of complexes, then it follows that

$$\begin{aligned} C &= \dim[\mathrm{im}(\mathbb{A})] + \dim[\ker(\mathbb{A})] \\ &= s + \delta + \dim[\ker(\mathbb{A})]. \end{aligned} \tag{38}$$

The expression for $\dim[\ker(\mathbb{A})]$ is simple and follows from the fact that $\mathbb{A}$ functions as an ordinary graph Laplacian on each connected component of the complexes. The argument involves the following observations.

Weak reversibility and linkage classes. Connected components in the simple graph that includes only complexes and reactions are termed linkage classes in the CRN literature. Weak reversibility is the condition that any node in a linkage class can be reached from any other by some sequence of reactions. The subset of complexes in a linkage class, which can be reached starting from any complex and which subsequently are never exited, is called a strong terminal linkage class. Weak reversibility of the whole CRN ensures that each linkage class is a strong terminal linkage class and (as in Ref. [10]) we will limit the discussion to this case for simplicity.[10]

The counting rule for deficiency. Weakly reversible processes are ergodic on each linkage class, so by the Perron-Frobenius theorem or an equivalent argument [11], there is one basis vector for $\ker(\mathbb{A})$ for each linkage class. Let l denote the number of linkage classes. Then $l = \dim[\ker(\mathbb{A})]$ and the Feinberg counting result that

$$\delta = C - s - l \tag{39}$$

follows from Eq. (38).

Complex-balanced steady states. Flows in $\ker(A)$ are termed complex balanced, because they require no net transport of flux to or from any complex to the species that make it up. All steady states must (tautologically) be in $\ker(Y\mathbb{A})$. If $\delta = 0$ the two spaces have the same dimension and thus are the same. In other words, the steady-state condition that there be no sources or sinks at species nodes entails the condition that there be no sources or sinks at complexes. In this case a convexity argument [9,11] implies that there is a unique steady state in the positive orthant for any value of the rate constants.

Nonzero deficiency. If $\delta > 0$ there are species-balancing flows that are not complex balancing and $\dim[\ker(\mathbb{A})]$ is larger than the number of constraints from $\partial n/\partial \tau = 0$ (which is only s). Steady states then generally exist out of the subspace of $\ker(\mathbb{A})$.

Using mean regression as a basis to decompose flows beyond the $\delta = 0$ condition

We noted above that a basis for $\ker(A)$ has one vector on each linkage class. At the level of individual linkage classes, these are profiles in Ψ proportional to the maximal eigenvectors of the Perron-Frobenius theorem for simple diffusion under $\mathbb{A}$. To characterize the remainder of the space of activities on the complexes, we require a basis that decomposes the preimage of the stoichiometric subspace from the remaining flows.

Let $\{e_\alpha\}_{\alpha=1}^{s}$ be a basis for $\ker(Y\mathbb{A})^\perp \subseteq \mathbb{R}^C$. Changes in Ψ along these directions lead to changes in flows $\partial n/\partial \tau$ within S, which we term s-flows. Let $\{\tilde{e}_\beta\}_{\beta=1}^{\delta}$ be a basis for $\ker(Y\mathbb{A})/\ker(\mathbb{A})$. Changes in Ψ along these directions lead to changes by species-balanced but not complex-balanced flows, which do not alter $\partial n/\partial \tau$ and which we term δ-flows. If follows that jointly $\{\{e_\alpha\}_{\alpha=1}^{s}, \{\tilde{e}_\beta\}_{\beta=1}^{\delta}\}$ form a basis for $\ker(\mathbb{A})^\perp \subseteq \mathbb{R}^C$.

This basis leads to a decomposition of $\mathbb{A}$ and therefore of $\mathcal{L}$, different from either the reaction or the complex representations in Eq. (3), which we might term the stoichiometric representation:

$$-\mathcal{L} = \psi_Y^\dagger \mathbb{A} \left\{ \sum_{\alpha=1}^{s} e_\alpha e_\alpha^\mathsf{T} + \sum_{\beta=1}^{\delta} \tilde{e}_\beta \tilde{e}_\beta^\mathsf{T} \right\} \psi_Y. \tag{40}$$

[9]These would be boundary solutions where some concentrations equal zero.

[10]The more general case differs only by superficial accounting to exclude complexes that are exited permanently.

The s-flows and δ-flows distinguished in the stoichiometric representation turn out to make dimensionally different contributions to the moment equations (34). The original Feinberg result, expressed in this language as saying that the s-flows completely determine the first-moment equations of motion (and that these are the only such flows for CRNs of deficiency zero), extends to a claim that the s-flows dominate the behavior of moments at all orders lower than the mean particle numbers, for general CRNs where they are not the only flows. We explore the consequences of these scaling dimensions in Sec. V.

B. Feinberg deficiency-zero theorem and the Anderson-Craciun-Kurtz theorem

Feinberg's deficiency-zero theorem was originally framed [9] as a result in the convex analysis of the mass-action rate law, which is generally assumed to be a mean-field approximation. The Anderson-Craciun-Kurtz theorem [24] uses the Feinberg existence proof for solutions to the mass-action rate law, but in proving that the underlying distributions have the form of a product of Poisson distributions (under the sampling model assumed throughout this paper), it actually strengthens Feinberg's original theorem: Because factorial moments of Poisson distributions have exactly the relation to the first moment assumed in mean-field formulations, the Feinberg solution to the mass-action rate equations need not be framed as a result in (unregulated) mean-field approximation, but can rather be seen as an exact result.

The Doi operator algebra, together with the stoichiometric decomposition in Eq. (40), provides an elegant way to both prove the ACK theorem and see that it makes the Feinberg theorem exact when $\delta = 0$ and also see why and how these results no longer hold when $\delta > 0$. We begin with the set of cases $\sum_p k_p = 1$ of Eq. (33), in which the sum on j contains the single term $j = k$; these are the equations of motion for the set of first moments. For species p,[11]

$$\begin{aligned}\frac{\partial}{\partial\tau}\langle N_p\rangle &= Y_p\mathbb{A}(0|\exp\left(\sum_q a_q\right)\psi_Y(a)|\phi)\\ &= Y_p\mathbb{A}\langle\Psi_Y(N)\rangle\\ &= Y_p\mathbb{A}\sum_{\alpha=1}^{s} e_\alpha e_\alpha^{\mathsf{T}}\langle\Psi_Y(N)\rangle.\end{aligned} \tag{41}$$

So far we work at general deficiency, but because $Y\mathbb{A}\tilde{e}_\beta \equiv 0\,\forall\beta$ by construction, only the basis elements corresponding to s-flows are nonzero.

Equation (41) is exact for this stochastic process and it is almost the same as the standard expression for the mass-action rate law, except that it involves an expectation of the observables $\Psi_Y(N)$, which may include higher-order correlations in N. Arbitrarily ignoring these correlations and replacing $\langle\Psi_Y(N)\rangle$ with $\psi_Y(\langle N\rangle)$ defines the mean-field approximation.

[11]Note how, from the symmetric form of $\mathcal{L}$ in Eq. (27), the asymmetry of the usual rate equations has resulted from the projection onto the dynamics of a particular moment.

The one case where the mean-field form is exact is when the state $|\phi)$ equals some coherent state $|\xi)$. The coherent states are the generating functions of Poisson distributions, constructed in the Doi algebra as

$$\begin{aligned}|\xi) &\equiv e^{(a^\dagger-1)\xi}|0)\\ &\leftrightarrow e^{(z-1)^{\mathsf{T}}\xi}\cdot 1 = e^{-1^{\mathsf{T}}\xi}\sum_{N_1}\cdots\sum_{N_P}\prod_p\frac{z_p^{N_p}\xi_p^{N_p}}{N_p!}.\end{aligned} \tag{42}$$

Here $\xi \equiv [\xi_p]$ is a vector of the mean particle numbers $\xi_p = n_p$ for the P chemical species.

Coherent states are eigenstates of the Doi lowering operator and thus

$$\psi_Y(a)|\xi) = \psi_Y(\xi)|\xi), \tag{43}$$

giving the mean-field form as an exact result

$$\langle\Psi_Y(N)\rangle = (0|\exp\left(\sum_q a_q\right)\psi_Y(a)|\xi) = \psi_Y(\xi) = \psi_Y(\langle N\rangle). \tag{44}$$

Using the basis $\{e_\alpha\}$ to handle the counting of dimensions in the stoichiometric subspace (not all linear combinations of n_p are necessarily dynamic in a particular CRN), the condition that $\partial n/\partial\tau = 0$ in Eq. (41) becomes

$$e_\alpha^{\mathsf{T}}\psi_Y(\xi) = 0 \quad \forall\alpha \in 1,\ldots,s. \tag{45}$$

These are the set of equations proved by Feinberg to have a unique, strictly positive solution when $\delta = 0$, for all nondegenerate values of the rate constants. Thus, if the distribution $|\phi)$ is a coherent state, the Feinberg result is an exact solution.

The coherent state identified by Eq. (45) is the ACK solution if it is a solution at all. However, whereas any mean-field equation can be solved for some coherent-state parameter, the corresponding state is only a solution to the whole moment hierarchy if it also leads to stasis of all higher moments. To see why this is ensured at $\delta = 0$ and not otherwise, we insert the stoichiometric decomposition (40) into the general moment hierarchy (34) to obtain

$$\begin{aligned}\frac{\partial}{\partial\tau}\left\langle\prod_p N_p^{\underline{k_p}}\right\rangle = &\sum_{j_1=0}^{k_1}\binom{k_1}{j_1}\cdots\sum_{j_P=0}^{k_P}\binom{k_P}{j_P}\left[\prod_p \dot{Y}_p^{\underline{j_p}}\right]\\ &\times\mathbb{A}\left\{\sum_{\alpha=1}^{s} e_\alpha e_\alpha^{\mathsf{T}} + \sum_{\beta=1}^{\delta}\tilde{e}_\beta\tilde{e}_\beta^{\mathsf{T}}\right\}\langle\Psi_{Y+(k-j)}(N)\rangle.\end{aligned} \tag{46}$$

On a coherent state, the vector of factorial moments $\langle\Psi_{Y+(k-j)}(N)\rangle$ differs from the value $\langle\Psi_Y(N)\rangle$ for the first-moment condition only by an overall factor $\prod_p \xi_p^{(k-j)_p}$. If $\delta = 0$, only s-flows are present in the decomposition and the set of projections $\{e_\alpha^{\mathsf{T}}\langle\Psi_{Y+(k-j)}(N)\rangle\} = \prod_p \xi_p^{(k-j)_p} \times \{e_\alpha^{\mathsf{T}}\langle\Psi_Y(N)\rangle\}$ vanishes exactly when Eq. (45) holds, for all values of k and j. Although the truncated factorials of stoichiometric coefficients $[\prod_p \dot{Y}_p^{\underline{j_p}}]$ generally differ from Y, this changes only the weight of the inner products with the e_α and thus the strength with which each s-flow contributes to the rate equation away from the steady state. Hence the coherent-state solution identified

by the first-moment condition (45) is a steady-state solution for the whole moment hierarchy, proving the ACK theorem.[12]

If $\delta > 0$, then δ-flows also exist in the sum (46). However, whereas $Y\mathbb{A}\tilde{e}_\beta \equiv 0\ \forall\beta$, $[\dot{\prod}_p Y_p^{\underline{j_p}}]$ will not generally project out $\mathbb{A}\tilde{e}_\beta$ in the higher-order terms $\sum_p j_p > 1$, except possibly in special cases of fine-tuning of the rate parameters. Therefore, in general, k-dependent linear combinations of $\tilde{e}_\beta^{\mathsf{T}}\langle\Psi_{Y+(k-j)}(N)\rangle$ and $e_\alpha^{\mathsf{T}}\langle\Psi_{Y+(k-j)}(N)\rangle$ will be required to vanish at a steady state, obviating any simple Poisson solution.

V. SCALING REGIMES, MATCHED ASYMPTOTIC EXPANSIONS, AND THE CONTROLLING ROLE OF MEAN-REGRESSING FLOWS

The series expansion in factorials of the stoichiometry from Eq. (34), together with the interpretation of each term as a projection operator for some product-Poisson distribution that we used to prove the ACK theorem in Sec. IV B, provides a way to associate different regions in the lattice of factorial moments with control by different subsets of the network flows. Both a set of practical solution methods for steady states, based on matched asymptotic expansions, and the concept of approximating a complex distribution locally by a product of Poisson distributions, follow when we recognize that different terms in the series expansion are associated with different scaling behaviors because they capture distinct combinations of the rate constants from the network.

The next three sections cover the following topics in order.

Descaling. We first introduce the descaling of the moment hierarchy with coherent-state parameters. Since for Poisson distributions these are the only scale parameters, descaling turns the moment hierarchy for a coherent state into a vector of 1's.[13]

Matched asymptotic expansions. Generalizing the Feinberg steady-state condition to all orders, as we did above to prove the ACK theorem, allows us to use the condition $\Lambda\Phi = 0$ as a recursion relation on k to solve the moment hierarchy, much like the solution of any Laplace equation, with Λ serving as the Laplacian on the lattice of moments. When we do this with the descaled moment hierarchy, it becomes easy to show that recursion upward in any component of k produces a convergent power-series expansion in the range $k/\xi \ll 1$ (where ξ stands for whichever particle number corresponds to the component of k being incremented), whereas recursion downward in k is convergent for $k/\xi \gg 1$. This suggests a general method of solution for moment hierarchies using matched asymptotic expansions, where the matching conditions are imposed in the region $k \sim \xi$.

The $1/n$ *expansion about Poisson backgrounds.* The same small-parameter recursion that controls the asymptotic expansion for $k/\xi \ll 1$ also shows a sense in which the mean-regressing flows (the s-flows) define a leading Poisson approximation to low-order moments for a general CRN. This is true even when the projection onto the basis $\{e_\alpha\}$ does not define a zero-deficiency subnetwork of the original CRN. We can construct a linear combination of the coherent-state solutions to the first-moment steady-state conditions for which the remainder term that must be added to obtain an exact solution makes a contribution that is $O(k/\xi)$ smaller than the contribution of the Poisson backgrounds for the low-order moments (those with $k/\xi \ll 1$).

A. Descaling the moment equations with coherent-state parameters

Just as Y_p projects out the ACK product of Poisson distributions for $\delta = 0$ networks, each of the projectors $[\dot{\prod}_p Y_p^{\underline{j_p}}]$ in the moment-recursion equation (34) projects out some product of Poisson distributions if values for the corresponding coherent-state parameters can be found. (If they are not unique, it can project out more than one such solution.) We may choose to reference exact solutions for Φ_k to locally chosen Poisson distributions in different regions of k corresponding to different terms $j \equiv [j_p]$ and let the recursion equations solve for the (smaller) deviations from these reference Poisson distributions.

For any vector $\xi \equiv [\xi_p]$ of mean values, we may descale the activities Ψ_Y^i from Eq. (23) as

$$\hat{\Psi}_Y^i(N) \equiv \prod_p \frac{N_p^{\underline{y_p^i}}}{\xi_p^{y_p^i}}. \tag{47}$$

If we normalize the Ψ_Y vectors in this way, a corresponding counternormalization of the adjacency matrix can be defined as

$$\hat{\mathbb{A}}_{ji} \equiv \mathbb{A}_{ji} \prod_p \xi_p^{y_p^i}. \tag{48}$$

In cases where we wish to use the stoichiometric representation (40), a similar descaling of the corresponding projection vectors is

$$\begin{aligned}
(\hat{e}_\alpha)_i &\equiv \frac{1}{\prod_p \xi_p^{y_p^i}}(e_\alpha)_i, \quad \left(\hat{e}_\alpha^{\mathsf{T}}\right)_i \equiv \left(e_\alpha^{\mathsf{T}}\right)_i \prod_p \xi_p^{y_p^i}, \\
(\hat{\tilde{e}}_\beta)_i &\equiv \frac{1}{\prod_p \xi_p^{y_p^i}}(\tilde{e}_\beta)_i, \quad \left(\hat{\tilde{e}}_\beta^{\mathsf{T}}\right)_i \equiv \left(\tilde{e}_\beta^{\mathsf{T}}\right)_i \prod_p \xi_p^{y_p^i}
\end{aligned} \tag{49}$$

for all α and β. All these are chosen so that

$$\begin{aligned}
\mathbb{A}\langle\Psi_Y(N)\rangle &\equiv \hat{\mathbb{A}}\langle\hat{\Psi}_Y(N)\rangle \\
&\equiv \hat{\mathbb{A}}\left\{\sum_{\alpha=1}^{s} \hat{e}_\alpha \hat{e}_\alpha^{\mathsf{T}} + \sum_{\beta=1}^{\delta} \hat{\tilde{e}}_\beta \hat{\tilde{e}}_\beta^{\mathsf{T}}\right\}\langle\hat{\Psi}_Y(N)\rangle.
\end{aligned} \tag{50}$$

Applying the scale transformations (47) and (48) to the equations of motion (34) for the moment hierarchy Φ gives the equation for a descaled hierarchy $\hat{\Phi}$, in which the leading

[12] This is the construction also found in [33].

[13] This is true as long as the descaling is done with the coherent state's own ξ values. More generally, the moment hierarchy becomes a geometric progression.

geometric dependence on ξ has been factored out:

$$\frac{\partial}{\partial\tau}\hat{\Phi}_k \equiv \frac{\partial}{\partial\tau}\left\langle\prod_p \frac{N_p^{\underline{k_p}}}{\xi_p^{k_p}}\right\rangle$$
$$= \sum_{j_1=0}^{k_1}\binom{k_1}{j_1}\cdots\sum_{j_P=0}^{k_P}\binom{k_P}{j_P}\left[\dot{\prod_p}\frac{Y_p^{\underline{j_p}}}{\xi_p^{j_p}}\right]\hat{\mathbb{A}}\langle\hat{\Psi}_{Y+(k-j)}(N)\rangle$$
$$\equiv \sum_{k'}\hat{\Lambda}_{kk'}\hat{\Phi}_{k'}. \tag{51}$$

Following Feinberg but extending his consideration to all moments, we try to construct steady states for which Eq. (51) can be used as a recursion relation among the moments of $\hat{\Phi}_k$.

B. Matched asymptotic expansions for the steady-state condition

The terms that govern the behavior of recursions in the components of k, if Eq. (51) is used to (exactly or approximately) solve for $\hat{\Phi}_k$, are combinations of the form

$$\binom{k}{j}\frac{Y^{\underline{j}}}{\xi^j} = \frac{k!}{(k-j)!\xi^j}\frac{Y^{\underline{j}}}{j!} \tag{52}$$

(with k, j, Y, and ξ carrying indices for each p, which we suppress to reduce clutter). The ratios $Y^{\underline{j}}/j!$ are fixed parameters of $\hat{\Lambda}$ and in any case only finite in number. The ratios that govern scaling behavior across the moment hierarchy are the terms $k!/(k-j)!\xi^j$. Because the stoichiometric coefficients and therefore the limits in the sums over j are finite, it is possible to consider a range of typical particle number $n \sim \xi \gg \max(j)$, in which $k!/(k-j)!\xi^j \sim (k/\xi)^j$ in the ranges that govern the transition between scaling regions. These scale factors govern the stability of asymptotic expansions as follows.

For any fixed value of k, increasing j in the sum (51) lowers the order of all moments in $\langle\hat{\Psi}_{Y+(k-j)}(N)\rangle$, at the same time multiplying the corresponding term by a coefficient $\sim(k/\xi)^j$. Let $\underline{j}$ be the smallest value at which $\dot{\prod}_p(Y_p^{\underline{j_p}}/\xi_p^{j_p})\hat{\mathbb{A}}$ does not vanish. (In general, this occurs when $\sum_q j_q = 1$, so exactly one of the terms $Y_p^{\underline{j_p}} = Y_p$ and $Y_q^{\underline{j_q}} = 1$ for all other $q \neq p$.)

To extend the recursion upward by one order, we must increment k while holding j fixed at $\underline{j}$. The new moments appearing at order k are referred to those at the immediately preceding order in the recursion by higher-order terms $j > \underline{j}$ in the sum at the current k. The relative magnitude of the preceding terms to the new terms scales as $\sim(k/\xi)^{j-\underline{j}}$. For $k \ll \xi$, successively higher-order terms are expressed as sums of lower-order terms with positive powers of k/ξ, consistent with both a nonzero radius of convergence and damping out of uncertainties in the initial conditions of the recursion. (The latter property is important for an asymptotic expansion to provide a robust solution algorithm.)

For $k \gg \xi$ the opposite is true: The lower-order terms must be solved as functions of the higher-order terms, which are multiplied by positive powers of ξ/k. Thus, in this range the downward recursion is consistent with a nonzero radius of convergence and damps out uncertainties in the starting conditions assumed at large k.

This argument is the basis for a solution in terms of matched asymptotic expansions, where stable recursions are carried out starting respectively from $k = 0$ (up-going) and from asymptotically large k (down-going), and matching conditions are imposed in the overlap region $k \sim \xi$, which are marginally stable for both series. An interesting feature of this solution is that, for CRNs where the mean-field approximation predicts multiple steady states, there may still be unique large-k asymptotic behaviors required to ensure boundedness of moments at all orders. In such cases, it is the downward recursion from large k that anchors the solution to the moment hierarchy. This is a counterintuitive result given the conventional mean-field approach to moment closure, which attempts to anchor all higher-order moments in solutions to the first moments, but as a consequence cannot obtain the ergodic sum over multiple steady states, which is a property of the exact all-orders solution.

We do not offer a formal proof that these asymptotic expansions can be consistently performed for all CRNs and all dimensionalities of the moment hierarchy, which is an exercise beyond the scope of the current paper. However, in one dimension, the recursion is elementary to define, and for higher-dimensional systems we offer examples of decompositions of the solution for which numerical simulation suggests that a similar expansion can be used.

C. Leading Poisson approximations to nonzero-deficiency CRNs

The above analysis of the scaling of terms in an asymptotic expansion for solutions to $\hat{\Lambda}\hat{\Phi} = 0$ has an immediate corollary: In general steady-state solutions, a basis of product-Poisson distributions associated with s-flows dominates the low-order moments. The kernel of the argument is that, although the projection operators associated with both s- and δ-flows share in the same scaling, at the lowest order where the upward-going recursion begins, the δ-flow contributions are projected out (recall that their absence from the first-moment conditions is their defining feature) therefore only s-flow contributions serve as seeds for the polynomial expansion in k/ξ. We now demonstrate that relation.

The steady-state condition for Eq. (51), with the stoichiometric decomposition inserted from Eq. (40), becomes

$$0 = \sum_{j_1=0}^{k_1}\binom{k_1}{j_1}\cdots\sum_{j_P=0}^{k_P}\binom{k_P}{j_P}\left[\dot{\prod_p}\frac{Y_p^{\underline{j_p}}}{\xi_p^{j_p}}\right]$$
$$\times\ \hat{\mathbb{A}}\left\{\sum_{\alpha=1}^{s}\hat{e}_\alpha\hat{e}_\alpha^{\mathsf{T}} + \sum_{\beta=1}^{\delta}\hat{\tilde{e}}_\beta\hat{\tilde{e}}_\beta^{\mathsf{T}}\right\}\langle\hat{\Psi}_{Y+(k-j)}(N)\rangle. \tag{53}$$

The lowest-k conditions that the moment hierarchy must satisfy are the first-moment conditions, which are the set of terms $\sum_q k_q = 1$ and $j = k$, for which exactly one $Y_p^{\underline{j_p}} = Y_p$

and $Y_q^{j_q} = 1$ for all other $q \neq p$, as noted in the preceding section.

Write the state vector $|\phi)$ for a general solution to Eq. (53) as a sum

$$|\phi) = \sum_\gamma c_\gamma |\xi^{(\gamma)}) + |\phi'), \tag{54}$$

in which $\{\xi^{(\gamma)}\}$ is the set of all mean-field solutions to the first-moment steady-state conditions and c_γ are coefficients to be determined. By construction $e_\alpha^\mathsf{T} \sum_\gamma c_\gamma \psi_Y(\xi^{(\gamma)}) = 0 \; \forall \alpha$.[14]

Refer to the corresponding expectations as

$$(0| \exp\left(\sum_q a_q\right) \psi_Y(a) c_\gamma |\xi^{(\gamma)}) \equiv \langle \Psi_Y(N) \rangle^{(\gamma)},$$
$$(0| \exp\left(\sum_q a_q\right) \psi_Y(a) |\phi') \equiv \langle \Psi_Y(N) \rangle' \tag{55}$$

and likewise for higher-order moments and descaled moments $\hat{\Psi}$.

Under the decomposition (54), the steady-state condition (53) becomes

$$\sum_{j_1=0}^{k_1} \binom{k_1}{j_1} \cdots \sum_{j_P=0}^{k_P} \binom{k_P}{j_P} \left[\prod_p \frac{Y_p^{j_p}}{\xi_p^{j_p}}\right] \hat{\mathbb{A}} \left\{\sum_{\alpha=1}^{s} \hat{e}_\alpha \hat{e}_\alpha^\mathsf{T} + \sum_{\beta=1}^{\delta} \hat{\tilde{e}}_\beta \hat{\tilde{e}}_\beta^\mathsf{T}\right\} \langle \hat{\Psi}_{Y+(k-j)}(N) \rangle'$$
$$= -\sum_\gamma \sum_{j_1=0}^{k_1} \binom{k_1}{j_1} \cdots \sum_{j_P=0}^{k_P} \binom{k_P}{j_P} \left[\prod_p \frac{Y_p^{j_p}}{\xi_p^{j_p}}\right] \hat{\mathbb{A}} \sum_{\beta=1}^{\delta} \hat{\tilde{e}}_\beta \hat{\tilde{e}}_\beta^\mathsf{T} \langle \hat{\Psi}_{Y+(k-j)}(N) \rangle^{(\gamma)}. \tag{56}$$

If there is a unique steady-state solution and if the descaled moment hierarchy $\hat{\Phi}$ is descaled with this ξ, then by construction it will be the case that $\langle \hat{\Psi}_{Y+(k-j)}(N) \rangle^{(\gamma)} = c_\gamma[1]$ (the vector of all 1's), for all k and j on the right-hand side of Eq. (56), which contains a single term in the sum on γ.[15] In the more general case, we can choose the descaling parameters so that $\langle \hat{\Psi}_{Y+(k-j)}(N) \rangle^{(\gamma)} = c_\gamma[1]$ for a particular γ of our choice. (Generally this means descaling whichever term makes the largest contribution on the right-hand side, to remove the k and j dependence in that term.) The argument that the term $|\phi')$ is subleading is then made in two steps.

(i) For some set of coefficients $\{c_\gamma\}$ we can ensure that $e_\alpha^\mathsf{T} \langle \Psi_Y(N) \rangle' = 0$. This is because the set of steady-state solutions for $\xi^{(\gamma)}$ form a basis for the set of all solutions to the first-moment steady-state conditions. In general (even if there is only one solution for ξ), the required coefficients $\{c_\gamma\}$ may need to be determined by matching conditions to a large-k asymptotic expansion.[16] [Note that the values of $\tilde{e}_\beta^\mathsf{T} \langle \Psi_Y(N) \rangle'$ are unconstrained at order $\sum_p k_p = 1$ and must be determined as part of the recursion on k.]

(ii) For $\sum_p k_p > 1$, the leading-order dependence on $\langle \hat{\Psi}_{Y+(k-j)}(N) \rangle^{(\gamma)}$ on the right-hand side of Eq. (56) comes when $\sum_p j_p = 2$ and by Eq. (52) this term is $O((k/\xi)^2 \langle \hat{\Psi}_{Y+(k-j)}(N) \rangle^{(\gamma)})$. The leading term on the left-hand side arises where $\sum_p j_p = 1$, involves only the s-flows, and is $O((k/\xi) \langle \Psi_{Y+(k-j)}(N) \rangle')$. Hence we conclude that, at the level of counting naive scaling dimensions, there is a perturbative expansion in small k/ξ about a sum of coherent states, in which $\langle \Psi_{Y+(k-j)}(N) \rangle' \sim O((k/\xi) \langle \hat{\Psi}_{Y+(k-j)}(N) \rangle^{(\gamma)})$. The reason it is meaningful to make such a scaling comparison, when the j values used to estimate the powers of scale factors are different on the left-hand and right-hand sides of Eq. (56), is that we have been free to choose the descaling parameter for $\hat{\Phi}$ so that for whichever γ gives the largest contribution, $\langle \hat{\Psi}_{Y+(k-j)}(N) \rangle^{(\gamma)} = c_\gamma[1]$, removing the k and j dependences from the source on the right-hand side of the equation.

This completes the argument.

VI. WORKED EXAMPLES

We now demonstrate the above results for moment hierarchies in a cascade of examples. Each successive example increases the generality of the problem and introduces a new feature of general solutions of CRNs. Explicit constructions involving transfer matrices or Liouville operators are given in the main text where they first occur and the corresponding forms that differ only by elaboration for later examples are deferred to Appendix A.

A. A CRN with one species, two states, and no conserved quantities

This model is a minimal nontrivial form for a CRN, showing how uniqueness of positive steady states follows from deficiency zero and exhibiting the proof of the ACK theorem in terms of coherent-state projection operators from Sec. IV B. The CRN is given by the graph introduced in Fig. 1 with the associated reaction scheme (1). Its mean-field rate equation is

$$\frac{\partial n}{\partial \tau} = \alpha n - \beta n^2. \tag{57}$$

[14]Note that $|\phi')$, as the generating function for a difference of distributions, will not generally be derived from any distribution with all positive values.

[15]Note that, even in the case of a unique steady state, we cannot presume that $c_\gamma = 1$ unless $\langle \Psi_Y \rangle$ includes a term proportional to $\Phi_0 \equiv \langle 1 \rangle$, because the first-moment condition does not otherwise fix the normalization of the geometric sequence within the total distribution.

[16]The monostable solution in Sec. VI B illustrates the need for a nontrivial normalization in the case of a unique solution and the bistable solution in Sec. VI C illustrates the case of a solution for a linear combination of Poisson backgrounds.

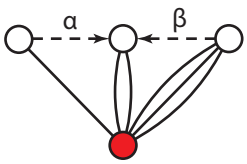

FIG. 2. Additional state added relative to the model of Fig. 1. This model is not weakly reversible.

The master equation, illustrating the decomposition (26) for the transfer matrix, is

$$\frac{\partial \rho_n}{\partial \tau} = [(e^{-\partial/\partial n} - 1)\alpha n + (e^{\partial/\partial n} - 1)\beta n(n-1)]\rho_n. \quad (58)$$

For the transfer matrix (58), the Liouville operator is

$$\begin{aligned}\mathcal{L} &= (1 - a^\dagger)(\alpha a^\dagger a - \beta a^\dagger a^2) \\ &= (1 - a^\dagger)(a^\dagger a)(\alpha - \beta a). \end{aligned} \quad (59)$$

The first line is a direct translation of the reaction representation from Eq. (3) for the conversion of particles in each unidirectional reaction. The second line extracts the overall factor of the projection operator $\alpha - \beta a$ that vanishes on a coherent state with parameter $\xi = \alpha/\beta$ in all moment equations, which is the proof of the ACK theorem given in Sec. IV B.

B. A CRN with one species, three states, and no conserved quantities

In this section we introduce a one-parameter family of models that have the same rate equation over the entire family. Figure 2 depicts a limiting member that lacks weak reversibility. Although the limiting case is formally outside the scope of the assumptions in the rest of the paper, it is useful to highlight the role of δ-flows in driving solutions away from the Poisson form associated with the ACK theorem. Weak reversibility may be established without changing the rate equation by adding two reactions to the graph of Fig. 2, to obtain the family (over the rate parameter ϵ) of graphs shown in Fig. 3, which we analyze below.

For this model, we demonstrate the stoichiometric decomposition of the Liouville operator from Eq. (40) and descaling of the moment recursion equation. For the parameters we will use in simulations, a single downward-going asymptotic expansion (obtained in [34]) is sufficient to solve the entire moment hierarchy to arbitrary precision, starting from an analytically derived large-k limiting form. However, we will also demonstrate the upward and downward matched asymptotic expansion to illustrate the stability properties of the recursion in small-k and large-k ranges. Exact solutions to moment hierarchies of this kind are only possible for birth-death [35] -type CRNs with one species, of which this class of models is an example, or for $\delta = 0$ CRNs, whereas the asymptotic expansions have a much wider applicability, as we demonstrate in later sections.

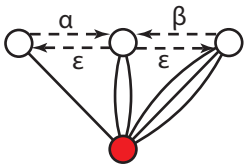

FIG. 3. Variant one-species model in which the complex graph is weakly reversible. The steady-state concentrations are the same as those in Fig. 2, which appear as a regular limit at $\epsilon \to 0$. Because $\delta = 1$, the distribution at the steady state is no longer Poissonian.

The rate equation for the CRNs in both Figs. 2 and 3 is

$$\frac{\partial n}{\partial \tau} = \alpha n - \beta n^3, \quad (60)$$

which differs from Eq. (57) only in changing the activities that govern particle creation and destruction. The simplest CRN graph with rate equation (60) is shown in Fig. 2, with the associated reaction scheme

$$A \overset{\alpha}{\rightharpoonup} 2A, \quad 2A \overset{\beta}{\leftharpoondown} 3A. \quad (61)$$

The model introduces competing autocatalysis at two orders: Particle creation occurs in proportion to the density of existing particles, while particle destruction occurs in proportion to the cube of the density. Because the CRN in Fig. 2 has only three complexes, however, the rate equation has only two nontrivial roots and therefore cannot support multiple positive steady states. (It does, however, have the marginally stable steady state $n \equiv 0$.)

The CRN of Fig. 3 with the reaction scheme

$$A \underset{\epsilon}{\overset{\alpha}{\rightleftharpoons}} 2A, \quad 2A \underset{\beta}{\overset{\epsilon}{\rightleftharpoons}} 3A \quad (62)$$

may be checked by Eq. (39) to have deficiency $\delta = 1$.

The master equation is provided in Eq. (A2) and the associated Liouville operator is

$$\begin{aligned}\mathcal{L} &= (1 - a^\dagger)[\alpha a^\dagger a - \epsilon(1 - a^\dagger)a^\dagger a^2 - \beta {a^\dagger}^2 a^3] \\ &= (1 - a^\dagger)(a^\dagger a)[(\alpha - \epsilon a) + (a^\dagger a - 1)(\epsilon - \beta a)]. \end{aligned} \quad (63)$$

The limit $\epsilon \to 0$ is degenerate with the graph of Fig. 2. The important feature of this Liouville operator is that the two projection terms $\alpha - \epsilon a$ and $\epsilon - \beta a$ are now multiplied by distinct nontrivial operators (respectively 1 and $a^\dagger a - 1$) and cannot both be made to vanish independently at a single Poisson solution at general values of ϵ. This is the way in which deficiency one (attained by adding a complex within a linkage class) moves the CRN outside the scope of the ACK theorem.

1. Stoichiometric decomposition

We can use the property suggested by the concept of deficiency, the categorization of flows as mean-regressing versus non-mean-regressing flows, to further clarify how the nonindependence of the projection terms in the Liouville operator (63) results in deviations from the Poisson steady-state form. The three decompositions of the Liouville operator

(63), from Eqs. (3) and (40), are given by

$$\begin{aligned}
\mathcal{L} &= \begin{bmatrix} a^\dagger & a^{\dagger 2} & a^{\dagger 3} \end{bmatrix} \left\{ \begin{bmatrix} 1 \\ -1 \\ 0 \end{bmatrix} \begin{bmatrix} \alpha & -\epsilon & 0 \end{bmatrix} + \begin{bmatrix} 0 \\ 1 \\ -1 \end{bmatrix} \begin{bmatrix} 0 & \epsilon & -\beta \end{bmatrix} \right\} \begin{bmatrix} a^1 \\ a^2 \\ a^3 \end{bmatrix} \\
&= \begin{bmatrix} a^\dagger & a^{\dagger 2} & a^{\dagger 3} \end{bmatrix} \left\{ \begin{bmatrix} 1 \\ 0 \\ 0 \end{bmatrix} \begin{bmatrix} \alpha & -\epsilon & 0 \end{bmatrix} + \begin{bmatrix} 0 \\ 1 \\ 0 \end{bmatrix} \begin{bmatrix} -\alpha & 2\epsilon & -\beta \end{bmatrix} + \begin{bmatrix} 0 \\ 0 \\ 1 \end{bmatrix} \begin{bmatrix} 0 & -\epsilon & \beta \end{bmatrix} \right\} \begin{bmatrix} a^1 \\ a^2 \\ a^3 \end{bmatrix} \\
&= \begin{bmatrix} a^\dagger & a^{\dagger 2} & a^{\dagger 3} \end{bmatrix} \frac{1}{\alpha^2+\beta^2} \left\{ \begin{bmatrix} \alpha^2 \\ -\alpha^2+\beta^2 \\ -\beta^2 \end{bmatrix} \begin{bmatrix} \alpha & 0 & -\beta \end{bmatrix} + \begin{bmatrix} 1 \\ -2 \\ 1 \end{bmatrix} \begin{bmatrix} \alpha\beta^2 & -\epsilon(\alpha^2+\beta^2) & \beta\alpha^2 \end{bmatrix} \right\} \begin{bmatrix} a^1 \\ a^2 \\ a^3 \end{bmatrix}
\end{aligned} \tag{64}$$

The first line is the reaction representation (since the reactions are bidirectional, we have combined both departure terms in the row vectors). The second line is the complex representation. In this representation it is clear why, if $\epsilon \to 0$, the reaction cannot be complex balanced: All terms in a given row vector have the same sign, so any positive density produces nonzero flows at some complexes. The last line is the stoichiometric representation. The first dyadic corresponds to the s-flow $\mathbb{A}ee^{\mathsf{T}}$ and the second dyadic corresponds to the δ-flow $\mathbb{A}\tilde{e}\tilde{e}^{\mathsf{T}}$.

Note that the diagonalization of the s-flow couples activity in the complex a to changes of probability across complexes $a^{\dagger 2}$ and $a^{\dagger 3}$ and vice versa with activity at a^3 and changes of probability across complexes $a^\dagger$ and $a^{\dagger 2}$. Thus, despite the similarity in form to the deficiency-zero projector in the Liouville operator from Eq. (59), the s-flow projection in Eq. (64) cannot be written as a stand-alone Liouville operator from a deficiency-zero subnetwork of the current network.

To illustrate the way in which different combinations of s- and δ-flows control the scaling of Φ_k in different regions, we note the forms of projection operators at different orders in the sum (34):

$$\begin{aligned}
&Y = Y^{\underline{1}} = [1 \quad 2 \quad 3], \quad Y^{\underline{1}}\mathbb{A} = [\alpha \quad 0 \quad -\beta], \quad Y^{\underline{2}} = [0 \quad 2 \quad 6], \quad \frac{Y^{\underline{2}}\mathbb{A}}{2!} = [\alpha \quad \epsilon \quad -2\beta], \\
&Y^{\underline{3}} = [0 \quad 0 \quad 6], \quad \frac{Y^{\underline{3}}\mathbb{A}}{6!} = [0 \quad \epsilon \quad -\beta].
\end{aligned} \tag{65}$$

The lowest-order term $Y^{\underline{1}}\mathbb{A}$ projects out solutions $\Phi_{k+2}/\Phi_k = \alpha/\beta$, while the highest-order term $Y^{\underline{3}}\mathbb{A}$ projects out the solution $\Phi_{k+2}/\Phi_{k+1} = \epsilon/\beta$. These turn out to be the two limiting moment ratios, respectively, in the limits $k = 1$ (the moment recursion formula has no term at $k = 0$) and $k \to \infty$, as we now demonstrate.

2. *Scaling behavior of the rate equation used as a recursion relation*

The Poisson background in the expansion (54), projected out by $Y^{\underline{1}}\mathbb{A}$ and ensuring vanishing of the s-flow contribution to the moment dynamics at each order k, is given by $\psi_Y = [\xi \quad \xi^2 \quad \xi^3]^{\mathsf{T}}$, where the mean number ξ satisfies

$$\xi^2 = \frac{\alpha}{\beta}. \tag{66}$$

This CRN has a unique steady state, so the terms appearing in Eq. (56) are

$$\begin{aligned}
k\frac{Y}{\xi}\hat{\mathbb{A}}\hat{e}\hat{e}^{\mathsf{T}}\langle\hat{\Psi}_{Y+(k-1)}(N)\rangle' &= \alpha k(\hat{\Phi}'_k - \hat{\Phi}'_{k+2}), \\
\sum_{j=2}^{k}\binom{k}{j}\frac{Y^{\underline{j}}}{\xi^j}\hat{\mathbb{A}}\{\hat{e}\hat{e}^{\mathsf{T}} + \hat{\tilde{e}}\hat{\tilde{e}}^{\mathsf{T}}\}\langle\hat{\Psi}_{Y+(k-j)}(N)\rangle' &= \frac{\alpha}{\xi}\frac{k!}{(k-2)!}\left\{(\hat{\Phi}'_{k-1} - \hat{\Phi}'_{k+1}) + \left(\frac{\epsilon}{\sqrt{\alpha\beta}}\hat{\Phi}'_k - \hat{\Phi}'_{k+1}\right)\right. \\
&\quad \left. + \left(\frac{k-2}{\xi}\right)\left(\frac{\epsilon}{\sqrt{\alpha\beta}}\hat{\Phi}'_{k-1} - \hat{\Phi}'_k\right)\right\}, \\
c_0\sum_{j=2}^{k}\binom{k}{j}\frac{Y^{\underline{j}}}{\xi^j}\hat{\mathbb{A}}\hat{\tilde{e}}\hat{\tilde{e}}^{\mathsf{T}}\hat{\psi}_Y(\xi) &= c_0\frac{\alpha}{\xi}\frac{k!}{(k-2)!}\left(1 + \frac{k-2}{\xi}\right)\left(\frac{\epsilon}{\sqrt{\alpha\beta}} - 1\right).
\end{aligned} \tag{67}$$

As the numerical evaluations below will show, this is a model in which, despite uniqueness of the Poisson solution matching the first and third moments, the overall normalization of the moment hierarchy is not anchored in the lowest term Φ_0, so a relative

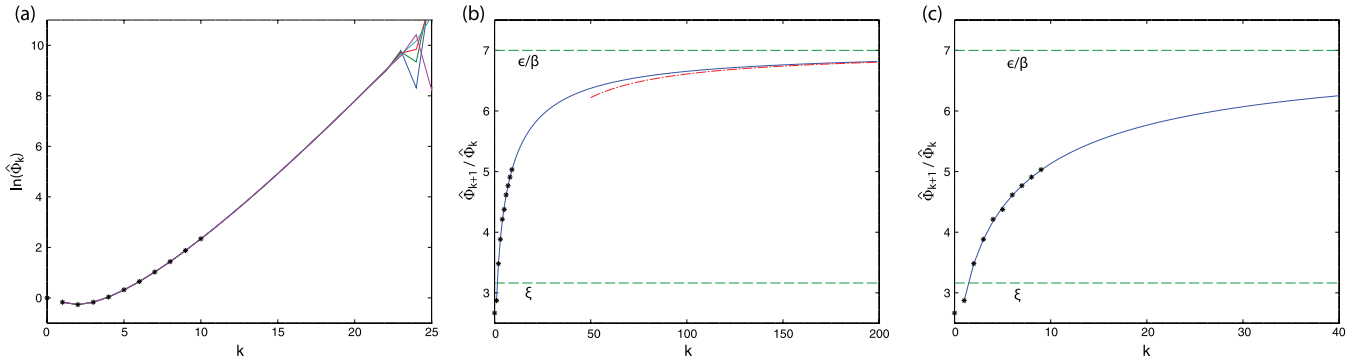

FIG. 4. Asymptotic expansions for moments and moment ratios for the model of Fig. 3. (a) Asymptotic expansion for $\ln \hat{\Phi}_k$ descaled with $\xi = \sqrt{\alpha/\beta}$ under the recursion relation (68), upward from $k = 1$. Five traces are generated by starting with $\langle N \rangle \equiv \langle N^3 \rangle$ fixed and $\langle N^2 \rangle$ values spaced by 1×10^{-10} around the stable value. The group of trajectories become uncontrollably divergent by $k = 25$. Asterisks are evaluations of the corresponding moments from a Gillespie simulation and the value of $\langle N \rangle$ was used to supply the unspecified normalization $c_0 \approx 2.67$ in Eq. (68) for the recursion series. (b) and (c), which differ only in the plotted range, show ratios $\hat{\Phi}_{k+1}/\hat{\Phi}_k$ (for which c_0 appears only in the lowest term $\langle N \rangle/1$). Curves computed by recursion downward from $k = 200$ with the starting approximation (69), shown as the red dash-dotted curve in (b). Gillespie simulation results overlaid as asterisks. The Poisson expectation ξ from MFT and the large-k asymptotic limit ϵ/β are shown as green dashed lines for reference.

normalization c_0 for the $\psi_Y(\xi)$ contribution is undetermined. In this way, the role of the Poisson background in an exact solution of the moment hierarchy is different from a mean-field approximation. Mean-field theory (MFT) would require $\langle N \rangle^2 = \alpha/\beta$ in place of Eq. (66), which requires $\langle N \rangle^2 = (c_0\xi)^2$. The freedom for ξ to differ from $\langle N \rangle$ by the normalization c_0 is necessary, because even for this simple network, the MFT prediction for the mean is not valid.

The exact recursion relation for the deviations from Poisson moments is then the finite sum

$$\hat{\Phi}'_k - \hat{\Phi}'_{k+2} + \frac{k-1}{\xi}\left\{(\hat{\Phi}'_{k-1} - \hat{\Phi}'_{k+1}) + \left(\frac{\epsilon}{\sqrt{\alpha\beta}}\hat{\Phi}'_k - \hat{\Phi}'_{k+1}\right) + \left(\frac{k-2}{\xi}\right)\left(\frac{\epsilon}{\sqrt{\alpha\beta}}\hat{\Phi}'_{k-1} - \hat{\Phi}'_k\right)\right\}$$
$$= -c_0\frac{k-1}{\xi}\left(1 + \frac{k-2}{\xi}\right)\left(\frac{\epsilon}{\sqrt{\alpha\beta}} - 1\right). \tag{68}$$

For parameters that produce suitably small mean particle number, the recursion relation implied by Eq. (68) may be solved for all k to any desired precision, from the upper asymptotic behavior alone, as shown in [34]. We are interested here, however, in understanding the small-k and large-k behaviors of the moments. To this effect, we can see directly both aspects of the scaling presented in Sec. V. As an asymptotic expansion, the recursion relation specifies the higher-order difference $\hat{\Phi}_{k+2} - \hat{\Phi}_k$ as a power series in k/ξ with coefficients from values and differences of Φ at lower k indices.

The seed for the expansion at orders $\hat{\Phi}'_4$ and higher from the Poisson background is the k-independent value $c_0(\epsilon/\sqrt{\alpha\beta} - 1)$, multiplied by a polynomial of $O(k/\xi)$. Note, however, that the terms $\hat{\Phi}'_2$ and c_0, which are undetermined by the first-moment condition $e^{\mathsf{T}}\langle \Psi_Y(N) \rangle = 0$, enter the recursion relation according to the scaling of the overall asymptotic expansion and are permitted to be $O(1)$ relative to $\epsilon/\sqrt{\alpha\beta} - 1$. Finally, we observe that for a fine-tuned value of the rate parameters $\epsilon = \sqrt{\alpha\beta}$, the correction term can be made to vanish and the ACK-like solution projected to zero by the s-flow term $\mathbb{A}ee^{\mathsf{T}}$ in Eq. (64) becomes a steady-state solution, even though for this CRN $\delta = 1$.

Next we illustrate how the asymptotic expansion with a requirement of boundedness at large k anchors the moment hierarchy at all orders. We seed the downward-going asymptotic expansion with the leading nonconstant approximation to the recursion relation around the limiting ratio projected out by $Y^3\mathbb{A}$ from Eq. (65), which has the form

$$\frac{\langle N^{\underline{k+1}} \rangle}{\langle N^{\underline{k}} \rangle} \approx \left(\frac{\epsilon}{\beta}\right)\left[1 - \frac{\epsilon^2 - \alpha\beta}{\epsilon\beta}\frac{1}{k-1}\right]. \tag{69}$$

The corresponding leading-order approximation for large-k moments may be written about any reference value k_0 as

$$\langle N^{\underline{k}} \rangle \approx \mathcal{N}\left(\frac{\epsilon}{\beta}\right)^k\left[1 - \frac{\epsilon^2 - \alpha\beta}{\epsilon\beta}\ln\left(\frac{k-1}{k_0}\right)\right]$$
$$\approx \mathcal{N}\left(\frac{\epsilon}{\beta}\right)^k\left(\frac{k_0}{k-1}\right)^{(\epsilon^2-\alpha\beta)/\epsilon\beta}, \tag{70}$$

where $\mathcal{N}$ is an overall normalization to be determined.

Figure 4 shows a comparison of the numerical regression from Eq. (68), both for an upward-going recursion from $k = 1$ and for a downward-going recursion with the large-k asymptotic seed (70), to estimates of the first ten moments from a Gillespie simulation of the underlying process. The parameters used in the demonstration are $\alpha = 100$, $\beta = 10$, and $\epsilon = 70$. So the relevant parameters are $\xi = \sqrt{\alpha/\beta} = \sqrt{10}$, $\epsilon/\beta = 7$, and $\epsilon/\sqrt{\alpha\beta} = \epsilon/\beta\xi \approx 2.2136$. We have normalized the constant c_0, which is unspecified by the recursion relation

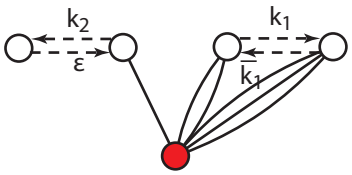

FIG. 5. This network, for some rate constants, can have two nonequilibrium steady states in the mean-field approximation. Even when this is the case, however, because the particle number is finite, the stochastic system always has only one ergodically sampled long-term steady distribution. Some subgraphs are common with Fig. 3, but the complex graph has two linkage classes, again giving $\delta = 1$.

to the simulated mean $\langle N \rangle$, and find close agreement with all other moment ratios.

C. A CRN with one species, four states, two linkage classes, and no conserved quantities

We can preserve the number of s-flows and δ-flows from the previous model, but introduce the possibility for multistability, by increasing both the number of complexes and the number of linkage classes by one. The resulting graph for a minimal model with this elaboration is shown in Fig. 5 and its reaction scheme is given by

$$\varnothing \underset{k_2}{\overset{\epsilon}{\rightleftharpoons}} A, \quad 2A \underset{\bar{k}_1}{\overset{k_1}{\rightleftharpoons}} 3A. \tag{71}$$

The corresponding rate equation is

$$\frac{\partial n}{\partial \tau} = \epsilon - k_2 n + k_1 n^2 - \bar{k}_1 n^3. \tag{72}$$

We have labeled the reaction rate constants in this model to reflect a set of cases that are often important in biochemistry and industrial synthesis: A reaction that is (directly or indirectly) self-catalyzed by feedback through the synthetic network is the main channel for production and decay of the product (rate constants k_1 and $\bar{k}_1$), compared to an uncatalyzed pathway that has nonzero but small rate ϵ, while a significant rate k_2 remains for spontaneous decay of the product. The scheme (71) is a slight generalization of the famous Schlögl model [41] to yield a weakly reversible complex network.

Quadratic-order autocatalysis in this CRN comes from the same pair of reactions as it does in Fig. 3. The addition of a fourth state to the complex graph creates a cubic first-moment rate equation and thus the possibility for multiple steady states.

For the graph of Fig. 5, the Liouville operator is

$$\begin{aligned}\mathcal{L} &= (1 - a^\dagger)[\epsilon - k_2 a + k_1 a^{\dagger 2} a^2 - \bar{k}_1 a^{\dagger 2} a^3] \\ &= (1 - a^\dagger)[(\epsilon - k_2 a) + (a^\dagger a)(a^\dagger a - 1)(k_1 - \bar{k}_1 a)]. \end{aligned} \tag{73}$$

The stoichiometric decomposition of this operator is similar to that from the previous model and is given in Eq. (A5).

The factorials $Y^{\underline{j}}$ and projection operators $Y^{\underline{j}}\mathbb{A}$ appearing in Eq. (34) are given by

$$\begin{aligned} Y &= Y^{\underline{1}} = [0 \quad 1 \quad 2 \quad 3], \\ Y^{\underline{1}}\mathbb{A} &= [\epsilon \quad -k_2 \quad k_1 \quad -\bar{k}_1], \\ Y^{\underline{2}} &= [0 \quad 0 \quad 2 \quad 6], \quad \frac{Y^{\underline{2}}\mathbb{A}}{2!} = 2[0 \quad 0 \quad k_1 \quad -\bar{k}_1], \\ Y^{\underline{3}} &= [0 \quad 0 \quad 0 \quad 6], \quad \frac{Y^{\underline{3}}\mathbb{A}}{3!} = [0 \quad 0 \quad k_1 \quad -\bar{k}_1]. \end{aligned} \tag{74}$$

The lowest-order (in k/ξ) projector in Eq. (74) is $Y^{\underline{1}}\mathbb{A}$, which is the projection operator corresponding to the s-flow in Eq. (A5). If required to vanish on a coherent state, it gives

$$\epsilon - k_2 \xi + k_1 \xi^2 - \bar{k}_1 \xi^3 = 0. \tag{75}$$

For appropriate parameter choices, this may have either a unique stable solution or three solutions, two stable and one between them that is unstable. Unlike the model of Fig. 3, both Φ_0 and Φ_2 have nonzero coefficients in $\langle \Psi_Y(N) \rangle$, so the normalization of the mean is fixed relative to $\Phi_0 \equiv 1$. Solutions of the form (54) must satisfy $\sum_\gamma c_\gamma = 1$ and therefore we may set $\langle \Psi_Y(N) \rangle' \equiv 0$.

In this model [contrasted with the result in Eq. (65)], both of the projection operators $Y^{\underline{2}}\mathbb{A}$ and $Y^{\underline{3}}\mathbb{A}$ cancel the same ratio $\Phi_{k+2}/\Phi_{k+1} = k_1/\bar{k}_1 \equiv K_1$, so there are only two scaling behaviors expressed in the model, respectively, at $k \to 0$ and $k \to \infty$. This CRN, also being a birth-death-type process, can be solved exactly [42] for the steady state. As for the three-state model, this moment hierarchy may also be solved by recursion from an upper asymptotic limit that is derivable analytically (though again the numerical calculation is stable only for sufficiently small mean particle numbers). If we define $\langle N^{\underline{k}} \rangle / \langle N^{\underline{k-1}} \rangle \equiv R_k$, then the set of R_k must obey the recursion

$$R_k = \frac{\epsilon + (k-1)(k-2)k_1}{k_2 - k_1 R_{k+1} + \bar{k}_1 R_{k+2} R_{k+1} - (k-1)(2k_1 - 2\bar{k}_1 R_{k+1}) + \bar{k}_1 (k-1)(k-2)}. \tag{76}$$

When we solve the recursion (76) numerically, directly in terms of moments Φ_k, we begin with a more refined large-k approximate form than the first-order approximation used as a seed in Eq. (69). The second-order leading nonconstant approximation, corresponding to the form (70) given for the previous model, is

$$\Phi_k \approx \mathcal{N} \left(\frac{k_1}{\bar{k}_1} \right)^k \left[1 + \frac{\eta}{k-1} + \frac{\eta(\eta/2 - K_1)}{k(k-1)} + O\left(\frac{1}{k^3} \right) \right], \tag{77}$$

where $\mathcal{N}$ is an arbitrary normalization to be fixed by $\Phi_0 = 1$ and

$$\eta \equiv \frac{k_2}{\bar{k}_1} - \frac{\epsilon}{k_1}. \tag{78}$$

The large-k asymptotic behavior of R_k in Eq. (76) can likewise be solved for an expansion in $1/k$ about the leading fixed point, in the same manner as Eq. (69) for the previous model. In this case, the leading departure is $O(1/k^2)$ rather

than $O(1/k)$ as in the three-complex model. In general, it can be shown that that the first departure from whatever fixed point is dictated by the leading large-k projection operator in Eq. (34) is determined by the highest power of k appearing in the expansion in the sum. This order corresponds to the largest stoichiometric coefficients for that component of k appearing in the CRN.

1. Bistability in MFT and handling mixtures of Poisson basis elements around $k = 0$

The handling of multistability in CRNs with $\delta > 0$ introduces several new interesting properties, both within the moment recursion relations and in their relation to mean-field theory. First, MFT will generally predict multistability for Poisson solutions, whether or not the mean particle number is large enough that trajectories in the stochastic process actually generate a multimodal density of particle numbers. The meaning of MFT solutions in relation to the analytic structure of representations of the generating function is an interesting topic from which we briefly draw results below, but mostly refer to other developments [36–38,43] (see also [44], Chap. 7). Second and more important, the moment relations are exact and we therefore expect them to possess unique solutions corresponding to the ergodic distribution, even when the mean particle number is large enough that the MFT representation of multistability corresponds to a true incipient[17] breaking of ergodicity. The expansion in high-order moments becomes an important if cryptic representation of the trajectories responsible for first-passages between domains.

We illustrate some of these properties for the case of bistability with a numerical example at the parameters $\epsilon = 36$, $k_2 = 49$, $k_1 = 14$, and $\bar{k}_1 = 1$. The two stable solutions to Eq. (75) are $\xi^{(1)} = 1$ and $\xi^{(3)} = 9$ and an unstable solution exists at $\xi^{(2)} = 4$.

Figure 6 shows the recursive solution for $\langle \hat{N}^{\underline{k}} \rangle$, descaled with $\xi^{(3)} = 9$, starting from the large-k asymptotic form (77). The solution exactly matches the expansion (54), with the coefficients given by

$$c_1 \approx 0.987, \quad c_2 \approx -0.092, \quad c_3 \approx 0.105. \tag{79}$$

Mean-field theory suggests no natural interpretation of the mixture (79) with a negative coefficient on an unstable solution. What would normally be done instead in MFT is to express the mean $\langle N \rangle \approx 1.56$ directly as a mixture of the two MFT stable values $\xi^{(1)} = 1$ and $\xi^{(3)} = 9$ with a mixing coefficient

$$c_{\text{eff}} \equiv \frac{\langle N \rangle - 1}{9 - 1} \approx 0.071. \tag{80}$$

[17]We say "incipient" because in conventional usage, breaking of ergodicity is an asymptotic property, here in the scaling variable $\langle N \rangle$ as $\langle N \rangle \to \infty$. Formally, ergodicity breaking can still be considered well defined even in finite-size systems, to the extent that it is associated with stationary paths in a semiclassical approximation that are essential singularities with respect to the asymptotic expansion in fluctuations [43].

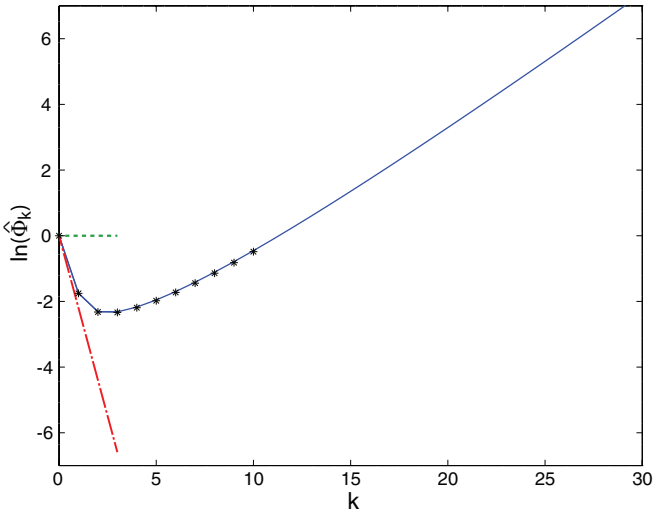

FIG. 6. Solution $\ln \hat{\Phi}_k$ to the recursion relations (33), descaled with $\xi^{(3)} = 9$, extended downward from $k = 200$ using the asymptotic approximation (77). The Poisson basis elements for $\xi^{(1)} = 1$ and $\xi^{(3)} = 9$ corresponding to the stable solutions in MFT are shown, respectively, as red dash-dotted and green dotted lines, for reference. The values $\hat{\Phi}_k$ for $k \in 0, \ldots, 3$ match an expansion (54) with the coefficients (79) and $\langle \Psi_Y(N) \rangle' \equiv 0$. Symbols are from a direct Gillespie simulation.

We will use the phenomenological description (80) to understand qualitatively how MFT and stationary-point expansions relate to the exact solution of the moment hierarchy.

2. Interpretation with a Kramers approximation for first-passage times

The interpretation of the ergodic solution in terms of a sum over naive mean-field backgrounds can be compared to a stationary-point expansion using the method of instantons, which is developed in [36,38,44]. Stationary-point locations and probabilities are governed by the minima of a nonequilibrium effective potential, which we have computed for this particular network in [45] (Chap. 7) and which takes the form[18]

$$\Xi(\bar{n}) = \int_4^{\bar{N}} dn \ln \left(\frac{k_2 n + \bar{k}_1 n^3}{\epsilon + k_1 n^2} \right). \tag{81}$$

The extrema of the effective potential are exactly the values of the Poisson parameters $\xi^{(\gamma)}$. (Here we arbitrarily set the zero of the effective potential to $n = 4$, the saddle point.) A plot of the effective potential versus n is shown in Fig. 7.

The probability to occupy either minimum may be approximated by the Kramers formula [46] derived from Ξ,

$$p_{\bar{n}} \propto \sqrt{\Xi''(\bar{n})} e^{-\Xi(\bar{n})}, \tag{82}$$

which follows from a semiclassical approximation to the escape rates by the nontrivial stationary trajectories known as instantons. Figure 7 shows that for these parameters, the

[18]In Ref. [45], we used the notation $\Phi(\bar{n})$ for the effective potential, which we change here to $\Xi(\bar{n})$ to avoid overlap with the notation for the moment hierarchy.

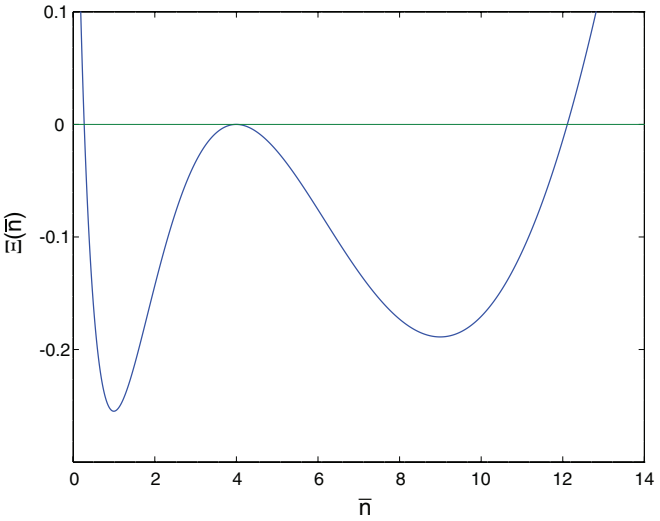

FIG. 7. Effective potential $\Xi(\bar{n})$ from Eq. (81).

minima of Ξ are approximately equal to -0.25 and -0.19, respectively, at $\bar{n} = 1$ and 9, so the Kramers approximation is not expected to be quantitatively accurate. The corresponding second derivatives Ξ'' take values approximately equal to 0.07 and 0.02.

Figure 8 shows a time series for the particle number N in a Gillespie simulation, with dashed lines indicating the minima of the effective potential (81). Some features of the stationary-point approximation are reflected: A majority of the time series remains near $N = \xi^{(1)} = 1$ with strong mean regression, while excursions with modest persistence and wider fluctuations occur out to $N \sim \xi^{(3)} = 9$. However, the excursions do not have the character of fully metastable equilibria. The logarithm of the empirical stationary distribution from the simulations is monotonically decreasing, with a visible shoulder (the signature that excursions are persistent) with a mode around $N \approx 15$.

Equation (82) gives, for the occupation probabilities of the two states, approximate values

$$p_{\bar{9}} \approx 0.20, \quad p_{\bar{1}} = (1 - p_{\bar{9}}) \approx 0.80, \tag{83}$$

in which $p_{\bar{9}}$ corresponds roughly to the empirical mixing coefficient c_{eff} in Eq. (80). The Kramers formula captures the larger weight on $\langle \Psi_Y(N) \rangle^{(1)}$, but overestimates the admixture of $\langle \Psi_Y(N) \rangle^{(3)}$ by about a factor of 3.

This CRN was also studied by Anderson *et al.* [42]. Using the fact that the steady-state probability ρ_{ss} is known, they showed that the nonequilibrium potential, defined here as $-\ln(\rho_{\text{ss}})$, converges to the Lyapunov function for the corresponding deterministic dynamics, in an appropriate scaling limit. The resulting Eq. (38) in [42] is our Eq. (81) obtained as a large-deviation function.

D. Two species, cross catalysis, and loss of factorability

The final model we will develop shows the loss, for $\delta > 0$, of the factorability that characterizes the steady states of deficiency-zero CRNs under the ACK theorem. We retain the properties already developed, of deviation from Poisson

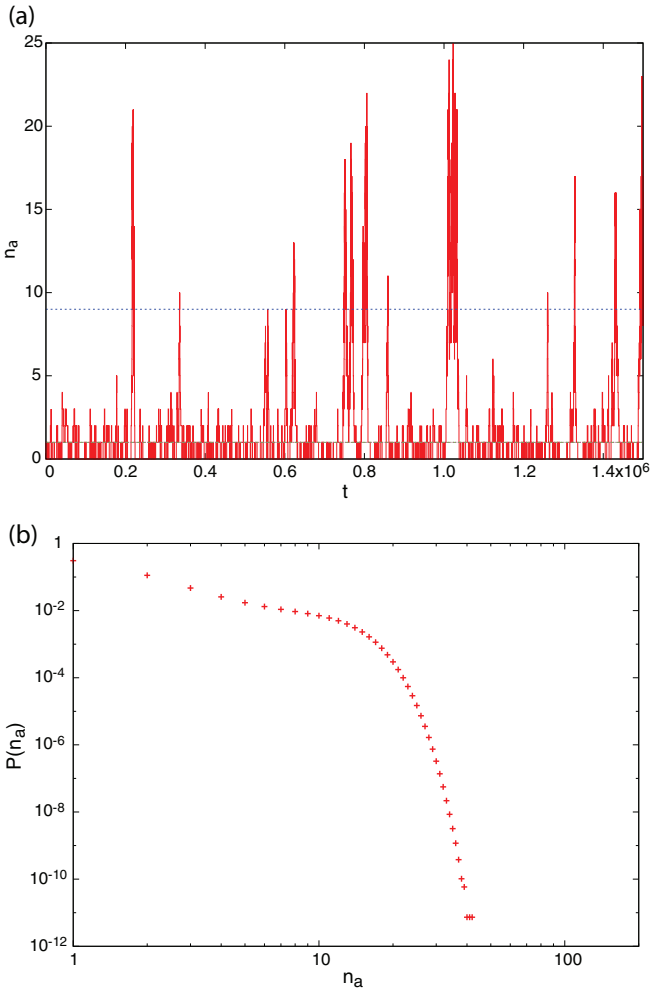

FIG. 8. (a) Time series for the particle number N in the four-state model of Fig. 5. Dotted lines label the minima of the effective potential (81) in the stationary-point expansion. (b) Histogram of the stationary distribution for N from the simulations, showing a monotonic decrease and a shoulder with a mode around $N \approx 15$.

statistics, and the capacity for multistability, by simply changing the autocatalytic feedback in the model of Fig. 5 to a cross-catalytic feedback between two symmetric chemical species.

The resulting multistable network, for two species A and B, is shown in Fig. 9 and its reaction scheme is given by

$$\begin{aligned} \varnothing &\underset{k_2}{\overset{\epsilon}{\rightleftharpoons}} A, \quad A + B \underset{\bar{k}_1}{\overset{k_1}{\rightleftharpoons}} 2A + B, \\ \varnothing &\underset{k_2}{\overset{\epsilon}{\rightleftharpoons}} B, \quad B + A \underset{\bar{k}_1}{\overset{k_1}{\rightleftharpoons}} 2B + A. \end{aligned} \tag{84}$$

The (now vector-valued) rate equation takes the form

$$\begin{aligned} \frac{\partial n_a}{\partial \tau} &= \epsilon - k_2 n_a + n_b\big(k_1 n_a - \bar{k}_1 n_a^2\big), \\ \frac{\partial n_b}{\partial \tau} &= \epsilon - k_2 n_b + n_a\big(k_1 n_b - \bar{k}_1 n_b^2\big). \end{aligned} \tag{85}$$

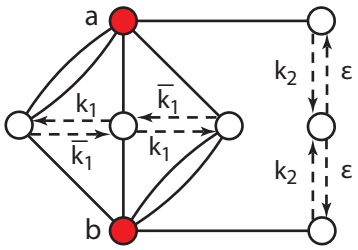

FIG. 9. This CRN uses two species in a cross-catalytic configuration to produce the same potential for bistability that the network of Fig. 5 produces through one-species autocatalysis. In this CRN $\delta = 2$ and the scaling behavior of each species separately is similar in many respects to one-species scaling of the network from Fig. 5.

The cross-catalytic CRN from Fig. 9 has the Liouville operator

$$\mathcal{L} = (1 - a^\dagger)[(\epsilon - k_2 a) + (b^\dagger b)(a^\dagger a)(k_1 - \bar{k}_1 a)] + (1 - b^\dagger)[(\epsilon - k_2 b) + (a^\dagger a)(b^\dagger b)(k_1 - \bar{k}_1 b)]. \quad (86)$$

We introduce pairs of raising and lowering operators $(a^\dagger, a)$ and $(b^\dagger, b)$, for the species A and B, respectively. The convention we adopt for ordering the components of the (somewhat complicated) vectors $\psi(a,b)$ and $\psi^\dagger(a^\dagger, b^\dagger)$ is given in Eq. (A6) and the corresponding stoichiometric decomposition of the Liouville operator is given in Eq. (A7).

1. Mean-field solutions and scaling regimes

The truncated factorials $Y_a^{\underline{j_a}}$ and $Y_b^{\underline{j_b}}$ that govern the scaling regimes in the steady-state moment hierarchy are provided in Eq. (A8). The lowest-order terms in the descaled form (51) of the moment equation are

$$\left(\frac{k_a}{\xi_a} Y_a e^{(k_a - 1)\partial/\partial Y_a} + \frac{k_b}{\xi_b} Y_b e^{(k_b - 1)\partial/\partial Y_b}\right) \hat{\mathbb{A}} \langle \hat{\Psi}_Y(N) \rangle. \quad (87)$$

The two vanishing conditions for $Y_a \hat{\mathbb{A}}$ and $Y_b \hat{\mathbb{A}}$ (coming from the projectors for the two s-flows of this network) are

$$(\epsilon - k_2 \xi_a) + \xi_a \xi_b (k_1 - \bar{k}_1 \xi_a) = 0,$$
$$(\epsilon - k_2 \xi_b) + \xi_a \xi_b (k_1 - \bar{k}_1 \xi_b) = 0. \quad (88)$$

These are solved at $\xi_a = \xi_b = \xi$, with ξ again satisfying the mean-field equation (75) for the single-species model of Sec. VI C.

In the other asymptote, the highest-order terms in Eq. (51) that are not identically zero in the componentwise product of $Y_a^{\underline{j_a}} \cdot Y_b^{\underline{j_b}}$ are

$$\frac{k_a k_b}{2\xi_a \xi_b} \left(\frac{k_a - 1}{\xi_a} Y_a^{\underline{2}} \cdot Y_b e^{-\partial/\partial Y_a} + \frac{k_b - 1}{\xi_b} Y_a \cdot Y_b^{\underline{2}} e^{-\partial/\partial Y_b}\right) \times \hat{\mathbb{A}} e^{(k_a - 1)\partial/\partial Y_a + (k_b - 1)\partial/\partial Y_b} \langle \hat{\Psi}_Y(N) \rangle. \quad (89)$$

The vanishing conditions for these two projectors are

$$\xi_a \xi_b (k_1 - \bar{k}_1 \xi_a) = 0,$$
$$\xi_a \xi_b (k_1 - \bar{k}_1 \xi_b) = 0. \quad (90)$$

They are again solved at $\xi_a = \xi_b = \xi$ but now with $\xi = k_1/\bar{k}_1 \equiv K_1$, reproducing the large-$k$ asymptotic condition from the single-species model of Sec. VI C.

This two-species case may again be solved for mixed moments in the neighborhood of the diagonal $k_a = k_b$, writing coupled recursion relations for the ratios of the factorial moments, as shown in [34]. In the following section we illustrate an alternate solution method using the asymptotic expansions that we have developed in the earlier sections.

2. Polynomial expansion of a solution for the moment equation in a neighborhood of the diagonal $k_a = k_b$

We now illustrate how the representation Λ of the generator for the stochastic process, acting similarly to a Laplacian on the two-dimensional lattice of moments $\Phi_{(k_a,k_b)}$, can be approximately solved in a neighborhood of the diagonal $k_a = k_b$. The method of solution is to use the symmetry of the recursion equations under $k_a \leftrightarrow k_b$ to expand solutions in even powers of $k_a - k_b$, with coefficient functions of $k_a + k_b$ solved by asymptotic expansion in a manner similar to that used in the one-species models of Secs. VI B and VI C.

The diagonal $k_a = k_b$ serves as an anchor for this approximation method, because it is also the contour of slowest approach for the classical mean-field solution.[19] Stabilization of a series solution in matched asymptotic expansions, for more complicated multidimensional stoichiometric subspaces in which the contour of slowest approach is nonaffine, is a challenging problem of a different kind, which falls outside the scope of our present treatment.

Even for the symmetric model, we do not have a proof that the radius of convergence of these solutions covers the entire lattice of k values, but comparisons to Gillespie simulation show good agreement in neighborhoods of the diagonal, suggesting that the asymptotic boundary conditions we use are consistent with those of full solutions. The existence of approximate solutions with this form shows a strong breaking of factorability from the form of products of Poisson distributions that is a characteristic of the ACK solution for deficiency-zero networks.

In the following solutions, two combinations of the rate constants that will appear repeatedly are given shorthand notation[20]

$$\omega \equiv \epsilon/k_1, \quad \eta \equiv k_2/\bar{k}_1 - \omega. \quad (91)$$

As in the asymptotic solutions for the one-species models, we begin by recognizing that the large-k asymptotic form is dominated by the scaling of the projection operator that is nonzero for the largest value of j in the sum (51). This is the projector given in Eq. (89). Therefore, we define the descaled

[19] The importance of contours of slowest approach was shown for a similar problem of the stabilization of instanton approximations in [36,47] and [38], Chap. 5.

[20] The second term η has already appeared in Eq. (78).

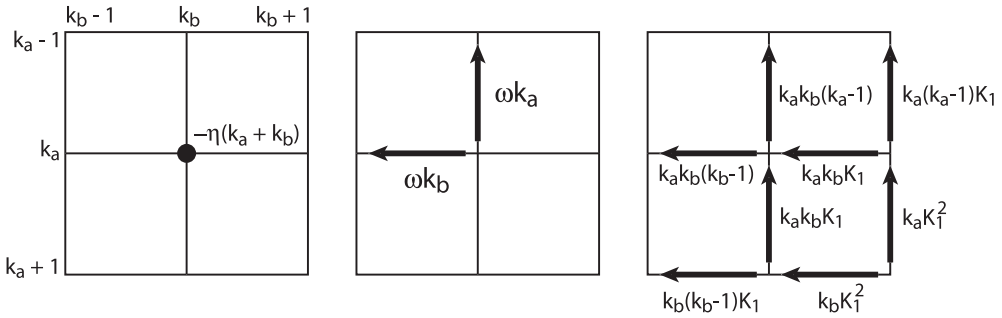

FIG. 10. Graphic representation of the action of the generator $\hat{\Lambda}$ given by Eq. (51) for the CRN of Fig. 9. The grid represents adjacent values of the index pair (k_a,k_b), $(k_a \pm 1,k_b)$, $(k_a,k_b \pm 1)$, and $(k_a \pm 1,k_b \pm 1)$, as indicated by axis labels in the first panel. The closed circle in the first panel represents multiplication by the moment at (k_a,k_b). Solid arrows indicate multiplication of moments by the projection vector $[1\ \ -1]$, acting on the moments at the tip and tail of the arrow. The labels on the lines indicate the function of parameters and k values that multiplies each such projector. Thus the first panel is simply the term $-\eta(k_a + k_b)\hat{\Phi}_{(k_a,k_b)}$, etc. The first and second panels, and the lower right pair of terms in the third panel, come from the terms at order $j_a + j_b = 1$ in Eq. (51), given in Eq. (87). The terms running antidiagonally through the center in the third panel come from the terms at order $j_a + j_b = 2$ and the terms in the upper left corner of the third panel come from the terms at order $j_a + j_b = 3$, shown in Eq. (89). The large-k asymptotic Poisson $\hat{\Phi} \to \mathcal{N}\underline{1}$ is annihilated identically by both panels with arrows.

moment operator by $\Phi_{(k_a,k_b)} \equiv K_1^{k_a+k_b}\hat{\Phi}_{(k_a,k_b)}$ and look for solutions in the form

$$\hat{\Phi}_{(k_a,k_b)} = \mathcal{N}\big[1 + \eta\varphi_{(k_a,k_b)}\big], \tag{92}$$

where $\varphi_{(k_a,k_b)} \to 0$ at large k_a or k_b.[21]

We introduce diagonal and transverse variables, written as functions of the vector argument k,

$$\kappa(k) \equiv k_a + k_b, \quad q(k)^2 = (k_a - k_b)^2. \tag{93}$$

In matrix multiplications below, we will often use κ and q^2 as function names, with the argument k, which is the index of summation suppressed as in usual matrix notation. We look for solutions to φ in the form of power series

$$\varphi = \sum_{\alpha=0}^{\infty} \varphi_\kappa^{(\alpha)} q^{2\alpha}. \tag{94}$$

Each term is to be chosen so that $\varphi_\kappa^{(\alpha)} \to 0$ as $\kappa \to \infty$. The functions $\varphi_\kappa^{(\alpha)}$ obey recursion relations similar to those for an infinite sequence of one-dimensional moment hierarchies labeled by α, except that the vectors in the sequence are coupled across values of α. Within the solution for each $\varphi_\kappa^{(\alpha)}$, we may treat κ itself as the discrete index of the recursion. Here, as in the one-species models, the descaled recursion relation suggests leading-order asymptotics for $\varphi_\kappa^{(\alpha)}$ in powers of $1/\kappa$, which may be used to seed numerical solutions.

The conversion from the original lattice $\hat{\Phi}_k$ to the sequence of vectors $\varphi_\kappa^{(\alpha)}$ leads to the following approximation procedure to solve for steady states: The steady-state condition from Eq. (51) is

$$0 = \hat{\Lambda}[\underline{1} + \eta\varphi] = \hat{\Lambda}\underline{1} + \eta\hat{\Lambda}\sum_{\alpha=0}^{\infty} \varphi_\kappa^{(\alpha)} q^{2\alpha}, \tag{95}$$

where $\underline{1} \equiv [1][1]^{\mathsf{T}}$ is the dyadic matrix of all 1's. We introduce a zeroth-order source term $s_\kappa^{(0)}$ defined by

$$\hat{\Lambda}\underline{1} = -\eta\frac{\kappa}{K_1} \equiv -\eta s_\kappa^{(0)}, \tag{96}$$

so the steady-state condition is equivalent to the series solution of an inhomogeneous Laplacian equation

$$\hat{\Lambda}\sum_{\alpha=0}^{\infty} \varphi_\kappa^{(\alpha)} q^{2\alpha} = s_\kappa^{(0)}, \tag{97}$$

in which $\hat{\Lambda}$ serves as Laplacian and $s_k^{(0)}$ is the source for the inhomogeneous solution.

The form of $\hat{\Lambda}$ can be described graphically in terms of difference operators acting across adjacent positions on the lattice of k values, as shown in Fig. 10. Here $\hat{\Lambda}$ acts nontrivially on $q^{2\alpha}$ as well as on $\varphi_\kappa^{(\alpha)}$, so Eq. (97) induces connections across orders in α and we relegate the details of a solution by successive approximations to Appendix B.

3. *Properties of steady states in the two-species model*

The major features of the steady-state solution in this model, which we have verified against Gillespie simulations, are the following.

Order of terms versus α. The naive scaling dimensions implied for $\varphi_\kappa^{(\alpha)}$ by Eq. (51) suggest that these functions should decay at large κ with increasing powers of $1/\kappa$. Numerically, this appears to be borne out, with indeed the entire series $\varphi_\kappa^{(\alpha)}$ decreasing in magnitude with increased α. In addition to the on-diagonal terms (where $q^2 \equiv 0$), which are defined entirely in terms of $\varphi_\kappa^{(0)}$, terms adjacent to the diagonal, which should be dominated by $\varphi_\kappa^{(\alpha)}$ at low orders in α, are well approximated by the solution $\varphi_\kappa^{(0)}$ across the whole range of $k_a = k_b$.

[21] We justify this assumed scaling by reference to the large-k limit (77) from the similar one-species model, because the orders of catalysis are more similar to that case than to the model of Sec. VI B leading to the soft (logarithmic) divergence of Eq. (70).

Scaling of finite-order approximations along rays of $|q|/\kappa$. The measure of error (nonzero values of $\partial\Phi_k/\partial\tau$) appears roughly constant along rays of fixed $|k_a - k_b|/(k_a + k_b) \equiv |q|/\kappa$ at finite orders of approximation in $\varphi_\kappa^{(\alpha)}$. Stabilizing the asymptotic expansion independently at each order of $\varphi_\kappa^{(\alpha)}$ becomes increasingly difficult as α increases, due to cross-level feedback and the successive-approximation algorithm we use for solution. Thus we obtain an approximate solution only through order $\varphi_\kappa^{(5)}$.

Comparison of the two-species cross-catalytic and one-species autocatalytic models. The ratios of adjacent moments in the value $k_a + k_b$, which require at minimum comparing on-diagonal and first off-diagonal moments, are shown in Fig. 11 and compared to the corresponding sequence of ratios derived from the moment solutions in Fig. 6. We find that the mean value $\langle N_a\rangle \equiv \langle N_b\rangle$ in the two-species model is very close to the mean value $\langle N\rangle$ from the one-species model, as suggested by the equivalence of their mean-field forms, even though both models differ significantly from the MFT approximation, which is the solution ξ to Eq. (75). Moreover, the second moments $\langle N_a N_b\rangle$ remain close to the one-species expectation $\langle N(N-1)\rangle$ and again different in both cases from the MFT prediction. At higher k, a different behavior is seen: The transition to scaling dominated by the term (89) is governed in the two-species model by k_a and k_b comparable to one-species k and not by the sum $k_a + k_b$. This is expected by comparing the forms of the two Liouville operators (73) and (86).

4. *Breaking of the factorability of the ACK theorem through cross catalysis*

The solution scheme defined in Sec. VI D 2 and worked out in Appendix B 1 suggests that the moment hierarchy near the diagonal is well approximated (at least at large k) by a function of $k_a + k_b$, which is a strong deviation from the factorability that would be produced by the ACK theorem for a deficiency-zero network. To study the failure of factorability more directly than through the numerical approximation scheme of Appendix B 1, we may alternatively approximate the large-k behavior of the moment hierarchy by a sum of products of powers of $1/k_a$ and $1/k_b$, solved fully for $\hat\Lambda\hat\Phi = 0$ order by order in $1/k$. The two expansions do not have the same asymptotics along the boundaries $k_a = 0$ and $k_b = 0$, but they can be made to satisfy the same boundedness criteria at large k in a neighborhood of $k_a = k_b$.

An expansion of the solution to $\hat\Lambda\hat\Phi = 0$ to second order in $1/k$ is given by

$$\begin{aligned}\Phi_{(k_a,k_b)} &\approx \mathcal{N}K_1^{k_a+k_b}\left[1 + \frac{\eta}{k_a + (K_1-\eta)/2} + \frac{\eta}{k_b + (K_1-\eta)/2} + \frac{\eta(\eta - K_1)}{[k_a + (K_1-\eta)/2][k_b + (K_1-\eta)/2]}\right]\\ &\approx \mathcal{N}K_1^{k_a+k_b}\left[\left(1 + \frac{\eta}{k_a + K_1/2} + \frac{\eta^2/2}{(k_a + K_1/2)^2}\right)\left(1 + \frac{\eta}{k_b + K_1/2} + \frac{\eta^2/2}{(k_b + K_1/2)^2}\right) - \frac{\eta K_1}{(k_a + K_1/2)(k_b + K_1/2)}\right],\end{aligned} \tag{98}$$

which we have checked numerically cancels the error term $\partial\hat\Phi/\partial\tau$ to the correct order of $1/k$.[22] The first departure from factorability occurs in the second-order term with numerator $-\eta K_1$, showing where the δ-flow contributions create correlated fluctuations that would be ruled out in a $\delta = 0$ network.

5. *Generalizing to a larger number of species*

Our constructions apply to CRNs with arbitrary numbers of species, but the foregoing models show how the character of solution methods changes with increasing numbers. Because the generator (34) has finitely many terms for any finite CRN, for one-species problems, the number of undetermined boundary data that must be sampled to search for stable asymptotic expansions is always finite. Moreover, the large-k limit may be extended to improve the precision of approximations from coarser seed functions. In two or more dimensions, unknown boundary data can exist along all surfaces of codimension 1 or more, in which one or more $k_p = 0$. If an asymptotic bounding surface is moved outward for the nonzero values of k_p, new unknown values are added to the set that must be sampled along small-k_p boundaries. Therefore, increasingly much of the information in a solution must come from boundary-condition data, compared to the constraint in the scalar condition $\Lambda\Phi = 0$.

Other problems of convex analysis, analogous to the Feinberg deficiency-zero argument, are also left as questions for future work. Is there a systematic way to represent the number of distinct scaling regions controlled by terms in the sum (34) over j? Do large-k asymptotic conditions on the vector ξ of coherent-state parameters always possess unique solutions? When are they underdetermined, and in these cases do the solutions from s-flow conditions extend outward indefinitely?

Despite leaving several detailed questions to be addressed, we emphasize that the finite rank of the operator Λ reduces the solving of a moment hierarchy to all orders, to a problem of equal complexity to solving a Laplacian diffusion equation, generally with beyond-nearest-neighbor couplings. This is a simpler and less-costly problem than direct simulation, especially for high-order moments in systems with large particle numbers.

[22] Equation (98) may be compared to Eq. (77) for the one-species model and also to the leading-order scaling estimate for the term $\varphi_\kappa^{(0)}$ from Eq. (B6). Along the diagonal $k_a = k_b$, Eq. (98) becomes $\Phi_{(k_a,k_b)} \approx \mathcal{N}K_1^{k_a+k_b}[\frac{4\eta(k_a+k_b)}{(k_a+k_b+K_1-\eta)^2}]$. The leading behavior differs from Eq. (B6) by a factor $4/3$ multiplying $K_1 - \eta$, which is consistent with the fact that the scaling solutions in Appendix B 1 only propagate the effects of $\hat\Lambda$ upward in a hierarchy of powers; feedbacks down the hierarchy are absorbed in higher-order correction terms that have the same large-k order as corrections in the multiplier of $K_1 - \eta$.

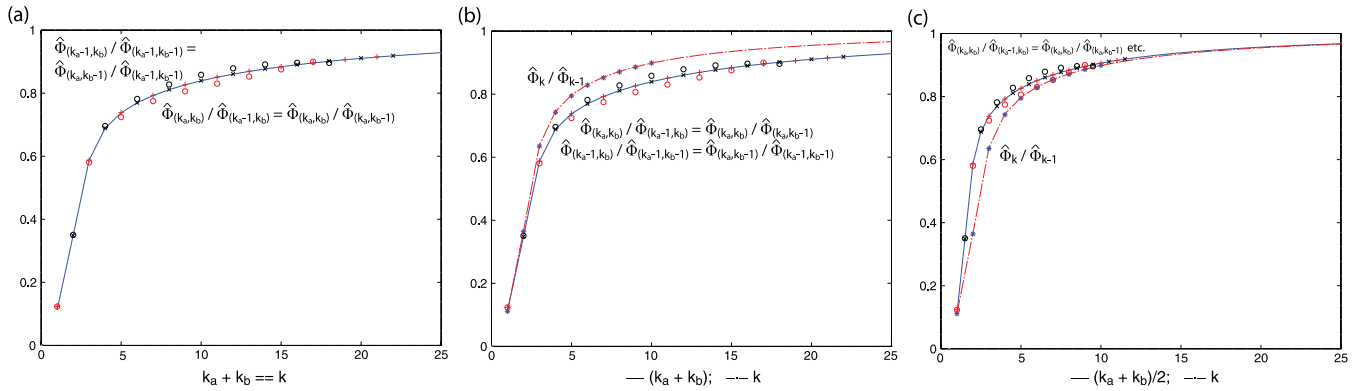

FIG. 11. Comparison of Gillespie simulations (circles) for the CRN model of Fig. 9 to the leading solution $\varphi_\kappa^{(0)}$ (solid curve and crosses) from Eq. (94). (a) Ratios $\hat{\Phi}_{(k_a,k_b)}/\hat{\Phi}_{(k_a-1,k_b)} = \hat{\Phi}_{(k_a,k_b)}/\hat{\Phi}_{(k_a,k_b-1)}$ for $k_a = k_b$ (black $\times$ and adjacent circles) and $\hat{\Phi}_{(k_a-1,k_b)}/\hat{\Phi}_{(k_a-1,k_b-1)} = \hat{\Phi}_{(k_a,k_b-1)}/\hat{\Phi}_{(k_a-1,k_b-1)}$ for $k_a = k_b$ (red + and adjacent circles). (b) and (c) Comparisons between these adjacent-moment ratios in the two-species model and moment ratios $\hat{\Phi}_k/\hat{\Phi}_{k-1}$ in the one-species model of Fig. 5 (red dash-dotted curve and asterisks) that has an equivalent MFT solution. (b) Plot of $k_a + k_b$ directly against one-species k, showing that for the lowest moments the total particle number controls similar moment values in the two models. (c) Plot of $(k_a + k_b)/2$ (equivalently, k_a or k_b) against one-species k, showing that the transition to scaling dominated by the autocatalytic reactions is governed independently by k_a and k_b.

VII. CONCLUSION

The observations and results of this work may be grouped under the following four main topics.

A shift in emphasis from topology to dynamics. In this article we have bypassed the use of deficiency as a topological index to categorize networks and focused instead on the contrast between mean-regressing and non-mean-regressing flows on the complex graph, which is the dynamical property that causes deficiency to be important. The dynamical distinction, which we express in the stoichiometric representation (40) of the stochastic-process generator, continues to be definable in terms of the images and kernels of $\mathbb{A}$ and $Y\mathbb{A}$, even in $\delta > 0$ networks where it cannot be associated with a deficiency-zero subnetwork. As shown in Sec. V C, the unique role of the mean-regressing flows as the determinants of the first-moment conditions, which persists to all orders in deficiency-zero networks, persists in a more limited form as the leading term in a $1/n$ expansion for the determination of moments in more general networks.

The Doi operator algebra, Laplace transforms, and an expanded role for Poisson basis distributions. The Doi operator algebra used to express the generators of the stochastic process is the tool that allows us to associate the s-flows and δ-flows in the stoichiometric representation with corresponding product-Poisson distributions, the origin and meaning of which are the same as those of the unique steady-state distributions in the Anderson-Craciun-Kurtz theorem. In this way, not only the linear algebra of first moments in the stoichiometric subspace, but the Poisson family of distributions as basis functions extends directly from deficiency-zero to deficiency-nonzero cases. This simplification and clarification results from working with the Laplace transform and the Liouville operator: The elementary projection operators in terms of which $\mathcal{L}$ naturally decomposes, which annihilate particular Poisson distributions, describe collective motions that recursively relate all orders in the moment hierarchy.

The manifestation of fundamental symmetries in the generator of the stochastic process. The Doi operator algebra also exposes symmetries of the generators (27) for stochastic CRNs that are obscured in the combination of index shifts and number dependence of rates in the master equation (26) and masked entirely in the asymmetric form of the mean-field mass-action rate equations (41) and (44). We use the simplifications this formalism affords to both derive the moment hierarchy and develop approximations to solve them.

Locality of scaling regions and connection to the Poisson approximations. The finiteness of the generator acting on the moment hierarchy is the feature that allows scaling regimes to be defined locally in different asymptotic ranges of moments and that makes Poisson-form basis distributions good approximations to the moment recursion relations in such regions. Despite the fundamental underlying complexity of CRNs–remember that the search for nonlocally defined topological properties such as shortest paths or feedback cycles can be NP-hard [13]—the convergence of both high- and low-k asymptotic expansions toward the matching region buffers the strength with which different regions are coupled and allows the convergence toward the Poisson basis elements to be locally governed. In this way, Poisson distributions that are among the lowest-information distributions serve as a basis for the evaluation of the moments in systems with the potential for very high information capacity. As a by-product, we also obtain a systematic approach to moment closure, which does not have any of the problems of *ad hoc* character and unphysical results [48] prevalent in existing schemes.

ACKNOWLEDGMENTS

E.S. thanks the Physics Department at Stockholm University for support during visits when the bulk of this work was carried out. We also acknowledge Dan Rockmore, Scott Pauls, and Greg Leibon for hospitality and conversations on related topics, Artur Wachtel, and Nathaniel Virgo of ELSI. E.S. acknowledges support from NASA Astrobiology CAN-7 award NNA17BB05A, and from the College of Science, Georgia Institute of Technology.

APPENDIX A: SUPPORTING ALGEBRA FOR CRN EXAMPLES

This appendix provides explicit forms for transfer matrices, Liouville operators, and truncated factorials of the stoichiometric matrix for the CRN models in the main text.

1. Forms of the transfer matrices appearing in master equations

Transfer matrices are given below for the indicated CRN models.

For the graph of Fig. 2 the evolution equation for the density that defines the transfer matrix has the form

$$\dot{\rho}_N = [(e^{-\partial/\partial N} - 1)\alpha N + (e^{\partial/\partial N} - 1)\beta N(N-1)(N-2)]\rho_N. \tag{A1}$$

This equation illustrates in the simplest form how Poisson steady states come to be ruled out when the ACK theorem no longer applies. The shift operator acts by single units $N \to N \pm 1$, but the numerical factors in the rates for particle creation and annihilation differ by second-order terms in N, which cannot be absorbed in any Poisson distribution.

For the weakly reversible graph of Fig. 3, the master equation adds a term affecting fluctuations though it preserves the first-moment rate equation

$$\dot{\rho}_N = \{(e^{-\partial/\partial N} - 1)[\alpha N + \epsilon N(N-1)] + (e^{\partial/\partial N} - 1)[\epsilon N(N-1) + \beta N(N-1)(N-2)]\}\rho_N. \tag{A2}$$

The master equation for the CRN of Fig. 5 is

$$\dot{\rho}_N = \{(e^{-\partial/\partial N} - 1)[\epsilon + k_1 N(N-1)] + (e^{\partial/\partial N} - 1)[k_2 N + \bar{k}_1 N(N-1)(N-2)]\}\rho_N. \tag{A3}$$

For the CRN of Fig. 9, N becomes a two-component index to ρ and the master equation becomes

$$\begin{aligned}\dot{\rho}_N = \{&(e^{-\partial/\partial N_a} - 1)[\epsilon + k_1 N_b N_a] + (e^{\partial/\partial N_a} - 1)[k_2 N_a + \bar{k}_1 N_b N_a(N_a - 1)] + (e^{-\partial/\partial N_b} - 1)[\epsilon + k_1 N_a N_b] \\ &+ (e^{\partial/\partial N_b} - 1)[k_2 N_b + \bar{k}_1 N_a N_b(N_b - 1)]\}\rho_N.\end{aligned} \tag{A4}$$

2. Stoichiometric representation forms for Liouville operators of the models

The stoichiometric decompositions of Liouville operators not explicitly written in the main text are provided here.

a. The one-species, four-complex model of Sec. VI C

The diagonalized form of the Liouville operator (73), corresponding to master equation (A3), is

$$\begin{aligned}\mathcal{L} = &\begin{bmatrix}1 & a^\dagger & a^{\dagger 2} & a^{\dagger 3}\end{bmatrix} \frac{1}{\epsilon^2 + k_2^2 + k_1^2 + \bar{k}_1^2} \left\{ \left((\epsilon^2 + k_2^2) \begin{bmatrix} 1 \\ -1 \\ 0 \\ 0 \end{bmatrix} + (k_1^2 + \bar{k}_1^2) \begin{bmatrix} 0 \\ 0 \\ 1 \\ -1 \end{bmatrix} \right) \begin{bmatrix}\epsilon & -k_2 & k_1 & -\bar{k}_1\end{bmatrix} \right. \\ &\left. + \begin{bmatrix} 1 \\ -1 \\ -1 \\ 1 \end{bmatrix} \left((k_1^2 + \bar{k}_1^2)[\epsilon \quad -k_2 \quad 0 \quad 0] - (\epsilon^2 + k_2^2)[0 \quad 0 \quad k_1 \quad -\bar{k}_1] \right) \right\} \begin{bmatrix} 1 \\ a \\ a^2 \\ a^3 \end{bmatrix}\end{aligned} \tag{A5}$$

in which the top line is the s-flow and the bottom line is the δ-flow.

b. The two-species, cross-catalytic model of Sec. VI D

For the two-species model of Fig. 9, the vectors of creation and annihilation operators with respect to which we will write $\mathcal{L}$ in matrix form are

$$\psi^\dagger = [1 \quad a^\dagger \quad b^\dagger \quad a^\dagger b^\dagger \quad a^{\dagger 2} b^\dagger \quad a^\dagger b^{\dagger 2}], \quad (\psi)^\mathsf{T} = [1 \quad a \quad b \quad ab \quad a^2 b \quad ab^2]. \tag{A6}$$

Then $\mathcal{L}$ from Eq. (86), corresponding to the master equation (A4), in matrix form and also diagonalized, becomes

$$\mathcal{L} = \psi^\dagger \left\{ \frac{1}{2(2\epsilon^2 + k_2^2 + 2k_1^2 + \bar{k}_1^2)} \left((2\epsilon^2 + k_2^2) \begin{bmatrix} 2 \\ -1 \\ -1 \\ 0 \\ 0 \\ 0 \end{bmatrix} + (2k_1^2 + \bar{k}_1^2) \begin{bmatrix} 0 \\ 0 \\ 0 \\ 2 \\ -1 \\ -1 \end{bmatrix} \right) \begin{bmatrix} 2\epsilon & -k_2 & -k_2 & 2k_1 & -\bar{k}_1 & -\bar{k}_1 \end{bmatrix} \right.$$

$$
\begin{aligned}
&+\frac{1}{2\left(k_2^2+\bar{k}_1^2\right)}\left(k_2^2\begin{bmatrix}0\\-1\\1\\0\\0\\0\end{bmatrix}+\bar{k}_1^2\begin{bmatrix}0\\0\\0\\0\\-1\\1\end{bmatrix}\right)[0\quad -k_2\quad k_2\quad 0\quad -\bar{k}_1\quad \bar{k}_1]\\
&+\frac{1}{2\left(2\epsilon^2+k_2^2+2k_1^2+\bar{k}_1^2\right)}\begin{bmatrix}2\\-1\\-1\\-2\\1\\1\end{bmatrix}\left(2k_1^2+\bar{k}_1^2\right)[2\epsilon\quad -k_2\quad -k_2\quad 0\quad 0\quad 0]-\left(2\epsilon^2+k_2^2\right)[0\quad 0\quad 0\quad 2k_1\quad -\bar{k}_1\quad -\bar{k}_1]\\
&+\frac{k_2\bar{k}_1}{2\left(k_2^2+\bar{k}_1^2\right)}\begin{bmatrix}0\\-1\\1\\0\\1\\-1\end{bmatrix}[0\quad -\bar{k}_1\quad \bar{k}_1\quad 0\quad k_2\quad -k_2]\Bigg\}\psi. \qquad \text{(A7)}
\end{aligned}
$$

The first line is the s-flow projected out by $a^\dagger a+b^\dagger b$; the second line is the s-flow projected out by $a^\dagger a-b^\dagger b$. The next two lines are the δ-flows with the same symmetry or antisymmetry. The stoichiometric vectors appearing in Eq. (51), and their products with $\mathbb{A}$ are

$$
\begin{aligned}
Y_a\equiv Y_a^1&=[0\quad 1\quad 0\quad 1\quad 2\quad 1],\quad Y_a^1\mathbb{A}=[\epsilon\quad -k_2\quad 0\quad k_1\quad -\bar{k}_1\quad 0],\\
Y_b\equiv Y_b^1&=[0\quad 0\quad 1\quad 1\quad 1\quad 2],\quad Y_b^1\mathbb{A}=[\epsilon\quad 0\quad -k_2\quad k_1\quad 0\quad -\bar{k}_1],\\
Y_a\cdot Y_b&=[0\quad 0\quad 0\quad 1\quad 2\quad 2],\quad (Y_a\cdot Y_b)\mathbb{A}=[0\quad 0\quad 0\quad 2k_1\quad -\bar{k}_1\quad -\bar{k}_1],\\
Y_a^2&=[0\quad 0\quad 0\quad 0\quad 2\quad 0]=Y_a^2\cdot Y_b,\quad Y_a^2\mathbb{A}=2[0\quad 0\quad 0\quad k_1\quad -\bar{k}_1\quad 0]=\left(Y_a^2\cdot Y_b\right)\mathbb{A},\\
Y_b^2&=[0\quad 0\quad 0\quad 0\quad 0\quad 2]=Y_b^2\cdot Y_a,\quad Y_b^2\mathbb{A}=2[0\quad 0\quad 0\quad k_1\quad 0\quad -\bar{k}_1]=\left(Y_b^2\cdot Y_a\right)\mathbb{A}. \qquad \text{(A8)}
\end{aligned}
$$

APPENDIX B: POLYNOMIAL EXPANSION FOR SOLUTIONS TO THE TWO-SPECIES CRN OF SEC. VI D

This Appendix describes the combination of the recursive solution and the successive approximation used to solve the hierarchical expansion (94) for the lattice of moments in the two-species model of Sec. VI D 2. Here, to simplify notation and improve readability, we will regard matrices such as $\hat{\Lambda}$ as operators that shift the indices (k_a,k_b) in terms $\varphi_k^{(\alpha)}q^{2\alpha}$ by means of discrete index-shift operators $e^{\partial/\partial k_a}$ and $e^{\partial/\partial k_b}$, as we did for transfer matrices in Eq. (26), etc. Because of the exchange symmetry in the dynamical equations under $k_a\leftrightarrow k_b$, $\hat{\Lambda}$ acts on $\varphi_k^{(\alpha)}$ through a shift of the κ value (by integers) and on $q^{2\alpha}$ through shifts in α. This allows us to treat κ as an index shifted by integers, analogous to k in single-species models. Where we suppress subscript κ indices, the whole vector is intended.

With these notational conventions, the action of the generator in Eq. (97) can be broken down into three terms

$$
\hat{\Lambda}(\varphi^{(\alpha)}q^{2\alpha})=(\hat{\Lambda}^0\varphi^{(\alpha)})q^{2\alpha}-s^{(\alpha+1)}q^{2(\alpha+1)}+\sum_{\beta=0}^{\alpha-1}\sigma_\beta^{(\alpha)}q^{2\beta}. \qquad \text{(B1)}
$$

Here $\hat{\Lambda}^0$ is a diagonal operator (in α) acting only on $\varphi^{(\alpha)}$, which takes the form (refer to Fig. 10)

$$
\begin{aligned}
(\hat{\Lambda}^0\varphi^{(\alpha)})_\kappa=&\left[\frac{(\kappa^2-\theta_{\alpha>0})(\kappa-2-2\alpha)-2\alpha\theta_{\alpha>0}}{4K_1}+\frac{\omega}{K_1}(\kappa-2\alpha)\right]\left(\varphi_{\kappa-1}^{(\alpha)}-\varphi_\kappa^{(\alpha)}\right)-\left[\kappa\left(\frac{\eta}{K_1}+2\alpha\right)+2\alpha\left(\frac{\omega}{K_1}-2\alpha\right)\right.\\
&\left.+\frac{2\alpha\kappa^2}{4K_1}+\theta_{\alpha>0}\frac{\kappa-2}{4K_1}\right]\varphi_\kappa^{(\alpha)}+[(\kappa-2\alpha)(\kappa-1)]\left(\varphi_\kappa^{(\alpha)}-\varphi_{\kappa+1}^{(\alpha)}\right)+\kappa K_1\left(\varphi_{\kappa+1}^{(\alpha)}-\varphi_{\kappa+2}^{(\alpha)}\right)-2\alpha K_1\varphi_{\kappa+1}^{(\alpha)}. \qquad \text{(B2)}
\end{aligned}
$$

In the same way as the action of $\hat{\Lambda}$ on the constant background $\underline{1}$ produced the zeroth-order source $-\eta s^{(0)}$ in Eq. (97), the action on each order $\varphi^{(\alpha)}$ generates a source term $s^{(\alpha+1)}$ in Eq. (B1) that propagates cross terms one order upward in α, defined by

$$
s_\kappa^{(\alpha+1)}=\frac{1}{4K_1}\left[(\kappa-2)\left(\varphi_{\kappa-1}^{(\alpha)}-\varphi_\kappa^{(\alpha)}\right)-2\alpha\varphi_{\kappa-1}^{(\alpha)}\right]. \qquad \text{(B3)}
$$

In addition to an upward-propagating source term, Eq. (B1) contains feedback terms, which propagate cross terms downward from order $q^{2\alpha}$ to all lesser orders $q^{2\beta}$ with $\beta < \alpha$, given by

$$\sigma_\beta^{(\alpha)} = \left[\kappa\binom{2\alpha}{2\beta} - \binom{2\alpha}{2\beta-1}\right]\left(\frac{\omega}{K_1}\varphi_{\kappa-1}^{(\alpha)} + [K_1 - (\kappa-1)]\varphi_{\kappa+1}^{(\alpha)}\right)$$
$$+ 2^{2(\alpha-\beta)}\left[\frac{\kappa(\kappa-2)}{2}\binom{2\alpha}{2\beta} - 2(\kappa-1)\binom{2\alpha}{2\beta-1} + 2\binom{2\alpha}{2\beta-2}\right]\varphi_\kappa^{(\alpha)}$$
$$+ \frac{1}{4K_1}\left\{\kappa^2\left[(\kappa-2)\binom{2\alpha}{2\beta} - \binom{2\alpha}{2\beta-1}\right] - \left[(\kappa-2)\binom{2\alpha}{2\beta-2} - \binom{2\alpha}{2\beta-3}\right]\right\}\varphi_{\kappa-1}^{(\alpha)}. \quad \text{(B4)}$$

In Eq. (B4), referring to the graphical form of Fig. 10, all terms from $j_a + j_b = 1$ are grouped in the first line, all terms from $j_a + j_b = 2$ are grouped in the second line, and all terms from $j_a + j_b = 3$ are grouped in the third line.

1. Solution by upward propagation in powers of q^2 and perturbative correction in $1/\kappa$

The decomposition (B1) of the steady-state condition can now be solved by alternating steps of exact cancellation of source terms at ascending orders in α and successive approximation to cancel feedback terms, which takes the form of a perturbative expansion in $1/\kappa$. Upward propagation consists of solving a series of Laplacian equations in the operator $\hat{\Lambda}^0$ in terms of the sources (B3) as

$$\hat{\Lambda}^0\varphi^{(\alpha)} = s^{(\alpha)} \quad \text{(B5)}$$

for all $\alpha \geqslant 0$.

Examination of the scaling terms in κ in Eq. (B2) suggests that a bounded large-κ asymptotic approximation for each order is

$$\varphi_\kappa^{(\alpha)} = \frac{4}{[\kappa + 4(K_1 - \eta)/3]^{2\alpha+1}} + O\left(\frac{1}{\kappa^{2\alpha+2}}\right). \quad \text{(B6)}$$

Solution of Eq. (B5) at each order α by a one-dimensional matched asymptotic expansion proceeds as for the one-species models. At order $\alpha = 0$, the solution can be stably extended down to $\kappa = 0$, but for $\alpha > 1$ the asymptotic approximation (B6) is not sufficient to produce convergence below $\kappa \sim 20$ and a nontrivial matched expansion is needed to produce valid higher-order corrections in q^2 to the low-order moments.

One round of forward propagation (through all orders α) will produce a solution that does not satisfy $\hat{\Lambda}\sum_{\alpha=0}^{\infty}\varphi^{(\alpha)}q^{2\alpha} - s^{(0)} = 0$, but rather

$$\hat{\Lambda}\sum_{\alpha=0}^{\infty}\varphi^{(\alpha)}q^{2\alpha} - s^{(0)} = \sum_{\alpha=0}^{\infty}\sum_{\beta=0}^{\alpha-1}\sigma_\beta^{(\alpha)}q^{2\beta}. \quad \text{(B7)}$$

The full solution can be approached perturbatively by using the feedback terms on the right-hand side of Eq. (B7) as sources for an iterative correction to the original φ.

Successive-approximation approach to full solutions $\varphi^{(\alpha)}$

A scaling analysis following from Eq. (B6) suggests that the correction terms needed to cancel the residuals in Eq. (B7) are suppressed by powers of $1/\kappa$ and thus that a method of successive approximations should converge. No feedback term $\sigma_0^{(\alpha)}$ to q^0 order from $\alpha = 0$ exists, because $\beta \leqslant \alpha - 1$ in the sum (B1). For all $\alpha \geqslant 1$, $\sigma_0^{(\alpha)}$ is given by

$$\left(\sigma_0^{(\alpha)}\right)_\kappa = \left(\frac{\omega\kappa}{K_1} + \frac{\kappa^2(\kappa-2)}{4K_1}\right)\varphi_{\kappa-1}^{(\alpha)} + \kappa[K_1 - (\kappa-1)]\varphi_{\kappa+1}^{(\alpha)}$$
$$+ 2^{2\alpha}\frac{\kappa(\kappa-2)}{2}\varphi_\kappa^{(\alpha)}. \quad \text{(B8)}$$

Since the lowest-order contribution is from $\varphi_\kappa^{(1)} \sim 4/\kappa^3$, it follows that $\sigma_0^{(\alpha)}$ is no larger for any α than the leading term

$$\left(\sigma_0^{(1)}\right)_\kappa = \frac{1}{K_1} + O\left(\frac{K_1}{\kappa^2}\right) + O\left(\frac{1}{\kappa}\right), \quad \text{(B9)}$$

one order lower (in either K_1 or κ, according to the range of κ) than the scaling of $s^{(0)}$ in Eq. (96). The same argument extends to higher β in Eq. (B7); the first term that contributes at each order scales with two additional powers of $1/\kappa$ and so is smaller than the corresponding $s^{(\alpha)}$ term in the first iteration of Eq. (B3).

We therefore introduce a second-order correction term $\varphi^{(\alpha)\prime}$, satisfying

$$\hat{\Lambda}\sum_{\alpha=0}^{\infty}\varphi^{(\alpha)\prime}q^{2\alpha} = -\sum_{\alpha=0}^{\infty}\sum_{\beta=0}^{\alpha-1}\sigma_\beta^{(\alpha)}q^{2\beta} + \sum_{\alpha=0}^{\infty}\sum_{\beta=0}^{\alpha-1}\sigma_\beta^{(\alpha)\prime}q^{2\beta}, \quad \text{(B10)}$$

where $\varphi^{(\alpha)\prime}$ is solved by upward propagation in $q^{2\alpha}$, as in Eq. (B5), but now with an entire tower of sources $-\sum_{\alpha=\beta+1}^{\infty}\sigma_\beta^{(\alpha)}$ at each order $q^{2\beta}$, rather than just the zeroth-order source $s^{(0)}$ that was used for $\varphi^{(\alpha)}$, and leaving its own residues $\sigma^{(\alpha)\prime}$. After infinitely many iterations, the residue terms go to zero as a sequence in powers of $1/\kappa$, and if the sequence converges, the sum over corrections will be a solution to the original steady-state condition (97).

An equivalent expression for the closed solution (summing over all orders of perturbative correction), expressed in terms of the homogeneous operator $\hat{\Lambda}^0$, is

$$\sum_{\alpha=0}^{\infty}(\hat{\Lambda}^0\varphi^{(\alpha)} - s^{(\alpha)})q^{2\alpha} = -\sum_{\alpha=0}^{\infty}\sum_{\beta=0}^{\alpha-1}\sigma_\beta^{(\alpha)}q^{2\beta}. \quad \text{(B11)}$$

Equation (B11) is similar in form to a Schwinger-Dyson equation for a Green's function solution, in which $\hat{\Lambda}^0\varphi^{(\alpha)} - s^{(\alpha)}$ serves as a bare Green's function, which defines a basis for perturbative incorporation of an interaction term $\sum_{\alpha=\beta+1}^{\infty}\sigma_\beta^{(\alpha)}$.

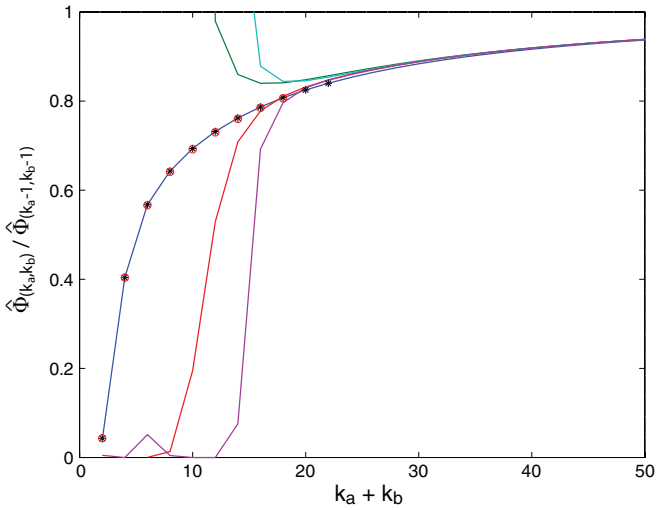

FIG. 12. Ratios of moments $\hat{\Phi}_{(k_a,k_b)}/\hat{\Phi}_{(k_a-1,k_b-1)}$ plotted versus $k_a + k_b \equiv k$, along the diagonal $k_a = k_b$. The series (94) is truncated at five successive orders of approximation $\varphi^{(\alpha_{\max})}$ for $\alpha_{\max} = 0, \ldots, 4$ (color sequence blue, green, red, cyan, magenta). Symbols are the ratios obtained directly from sampled moments of a stationary Gillespie simulation, showing that the order $\alpha_{\max} = 0$ provides a good approximation to the diagonal moments, as shown in Fig. 11. Divergence of higher-order terms, which occurs with opposite sign for odd versus even $\alpha_{\max}$, reflects instability of the asymptotic expansion downward from large κ.

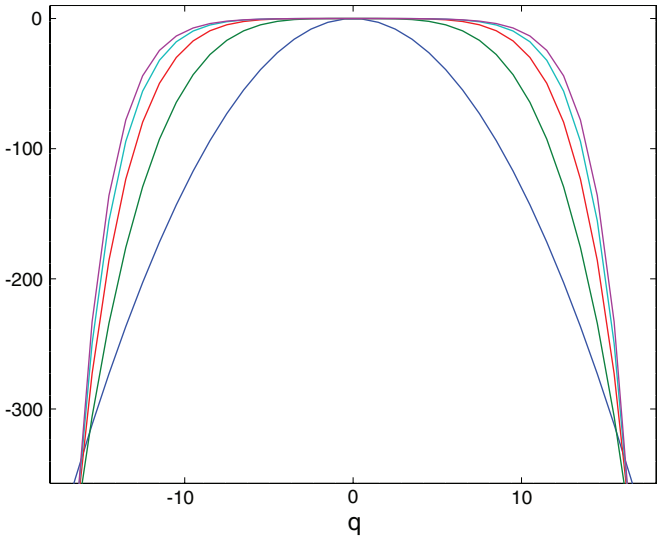

FIG. 13. Graph of the residual error measure $\partial\hat{\Phi}_{(k_a,k_b)}/\partial\tau$ across the contour $k_a + k_b = 49$, with the series (94) truncated at five successive orders of approximation $\varphi^{(\alpha_{\max})}$ for $\alpha_{\max} = 0, \ldots, 4$ (color sequence blue, green, red, cyan, magenta). Under perfect cancellation, the residual error at each order $\alpha_{\max}$ would scale as $q^{2(\alpha_{\max}+1)}$. This scaling is very closely approximated for $\alpha_{\max} = 1$ and degrades due to imperfect control of asymptotic expansions at higher orders, though the approximate behavior is attained. Crossing of the error curves suggests a finite radius of convergence in q^2 of the series (94), for $|q|/\kappa \sim 0.38$. The asymptotic expansion remains this good or better for all larger κ.

2. Numerical evaluations

We have implemented the above solution method for a series (94) truncated at five successive orders of approximation $\varphi^{(\alpha_{\max})}$ for $\alpha_{\max} = 0, \ldots, 4$. Under perfect convergence of the perturbative recurrence (B10), the error measure $\partial\hat{\Phi}_{(k_a,k_b)}/\partial\tau$ would cancel to order $q^{2(\alpha_{\max}+1)}$ around the diagonal (order q^{10} for the highest-order approximation we compute). We obtain cancellation along the diagonal to machine precision for the lowest-order correction $\varphi^{(0)}$, but instability of the downward-going asymptotic expansion at higher orders degrades both the accuracy of $\hat{\Phi}_{(k_a,k_b)}$ on the diagonal for $k_a + k_b \lesssim 20$ and convergence toward the $q^{2(\alpha_{\max}+1)}$ residual.

Figure 12 shows the successive approximations to the ratio $\hat{\Phi}_{(k_a,k_b)}/\hat{\Phi}_{(k_a-1,k_b-1)}$ along the diagonal $k_a = k_b$, compared to values obtained from a Gillespie simulation. The approximation $\alpha_{\max} = 0$ already shows good agreement with simulations. Divergence of the downward-going asymptotic expansion for higher-order terms begins around $k_a = k_b \approx 9$, which is the upper stable solution for the coherent-state mean number (75), as predicted in the scaling analysis of Sec. V B.

Figure 13 shows the error measure $\partial\hat{\Phi}_{(k_a,k_b)}/\partial\tau$ (the deviation from a full steady-state condition) across the antidiagonal contour $k_a + k_b = 49$, testing the quality of the convergence of the $\varphi^{(\alpha_{\max})}$ approximation. This contour is in a range $k_a, k_b \gg 9$ where the asymptotic expansions are still fairly well controlled. The qualitative character of the convergence is well approximated along the diagonal, but exact cancellation to order $q^{2(\alpha_{\max}+1)}$ degrades at higher $\alpha_{\max}$, as both the asymptotic expansion and the recursive solution (B10) accumulate numerical errors. The figure also shows the crossing of error contours at $|q|/\kappa \sim 0.38$, suggesting a finite radius of convergence that does not cover the entire (k_a, k_b) lattice.

Figure 14 is a contour plot of the errors $\partial\hat{\Phi}_{(k_a,k_b)}/\partial\tau$ for $\alpha_{\max} = 5$. The antidiagonal cross section corresponds to

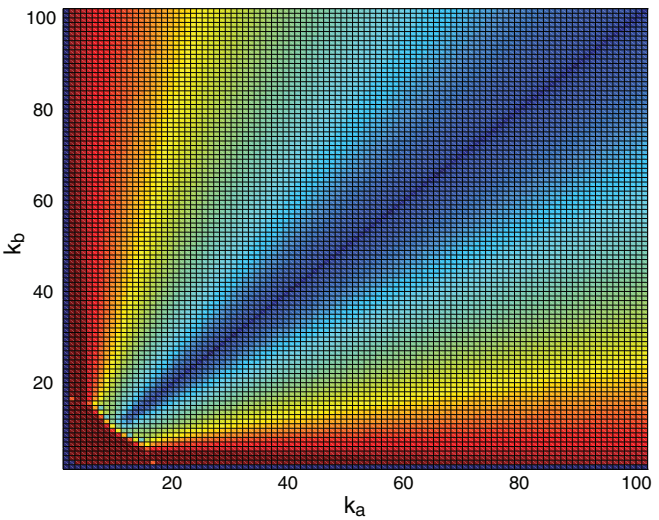

FIG. 14. Linear color map of the error function $\partial\hat{\Phi}_{(k_a,k_b)}/\partial\tau$ for $\alpha_{\max} = 5$, evaluated as the left-hand side of Eq. (95), which would equal zero for a stationary distribution. The deviation from zero is raised to the 0.1 power to produce a linear cross section if the true residuals scale as q^{10}.

the outermost curve from Fig. 13, raised to the 0.1 power appropriate if the total error scales as q^{10}. The region $k_a + k_b \lesssim 20$ shows the divergence of the asymptotic expansions already noted in Fig. 12. In the region where the asymptotic expansions converge, the errors are roughly constant along contours of fixed $|q|/\kappa$ for large k.

[1] L. László, Random walks on graphs: A survey, Bolya Math. Stud. **2**, 1 (1993).

[2] B. Luo, R. C. Wilson, and E. R. Hancock, Spectral embedding of graphs, Pattern Recogn. **36**, 2213 (2003).

[3] A. B. Lee and L. Wasserman, Spectral connectivity analysis, J. Am. Stat. Assoc. **105**, 1241 (2008).

[4] W. Hordijk and M. Steel, Detecting autocatalytic, self-sustaining sets in chemical reaction systems, J. Theor. Biol. **227**, 451 (2004).

[5] V. Danos, J. Feret, W. Fontana, R. Harmer, and J. Krivine, in *Formal Methods in Systems Biology*, edited by J. Fisher, Lecture Notes in Computer Science Vol. 5054 (Springer, Berlin, 2008), p. 103.

[6] R. Harmer, V. Danos, J. Feret, J. Krivine, and W. Fontana, Intrinsic information carriers in combinatorial dynamical systems, Chaos **20**, 037108 (2010).

[7] J. L. Andersen, C. Flamm, D. Merkle, and P. F. Stadler, Inferring chemical reaction patterns using rule composition in graph grammars, J. Syst. Chem. **4**, 14 (2013).

[8] J. L. Andersen, C. Flamm, D. Merkle, and P. F. Stadler, Generic strategies for chemical space exploration, Int. J. Comput. Biol. Drug Des. **7**, 225 (2014).

[9] M. Feinberg, Lectures on chemical reaction networks, The Ohio State University, 1979, available at https://crnt.osu.edu/LecturesOnReactionNetworks.

[10] J. Gunawardena, Chemical reaction network theory for *in-silico* biologists, lecture notes, Harvard University, 2003, available at vcp.med.harvard.edu/papers/crnt.pdf.

[11] J. C. Baez and J. D. Biamonte, Quantum techniques for stochastic mechanics, University of California, Riverside, 2017, available at math.ucr.edu/home/baez/stoch_stable.pdf.

[12] C. Berge, *Graphs and Hypergraphs* (North-Holland, Amsterdam, 1973).

[13] J. L. Andersen, C. Flamm, D. Merkle, and P. F. Stadler, Maximizing output and recognizing autocatalysis in chemical reaction networks is NP-complete, J. Syst. Chem. **3**, 1 (2012).

[14] D. E. Metzler, *Biochemistry: The Chemical Reactions of Living Cells*, 2nd ed. (Academic, New York, 2003).

[15] B. O. Palsson, *Systems Biology* (Cambridge University Press, Cambridge, 2006).

[16] H. L. Smith and H. R. Thieme, *Dynamical Systems and Population Persistence* (American Mathematical Society, Providence, 2011), Vol. 118.

[17] L. J. S. Allen, *An Introduction to Stochastic Processes with Applications to Biology* (Pearson, Cranbury, 2003).

[18] M. Feinberg, Chemical reaction network structure and the stability of complex isothermal reactors—I. The deficiency zero and deficiency one theorems, Chem. Eng. Sci. **42**, 2229 (1987).

[19] G. Craciun and M. Feinberg, Multiple equilibria in complex chemical reaction networks, SIAM J. Appl. Math **65**, 1526 (2005).

[20] G. Craciun, Y. Tang, and M. Feinberg, Understanding bistability in complex enzyme-driven reaction networks, Proc. Natl. Acad. Sci. USA **103**, 8697 (2006).

[21] H. Ji, Uniqueness of equilibria for complex chemical reaction networks, Ph.D. thesis, The Ohio State University, 2011.

[22] B. Joshi and A. Shiu, A survey of methods for deciding whether a reaction network is multistationary, Math. Model. Nat. Phenom. **10**, 47 (2015).

[23] M. R. Evans and T. Hanney, Non-equilibrium statistical mechanics of the zero-range process and related models, J. Phys. A: Math. Gen. **38**, R195 (2005).

[24] D. F. Anderson, G. Craciun, and T. G. Kurtz, Product-form stationary distributions for deficiency zero chemical reaction networks, Bull. Math. Biol. **72**, 1947 (2010).

[25] F. P. Kelly, *Reversibility and Stochastic Networks* (Wiley, Chichester, 1979).

[26] F. Horn and R. Jackson, General mass action kinetics, Arch. Rat. Mech. Anal **47**, 81 (1972).

[27] U. Seifert, Stochastic thermodynamics fluctuation theorems, and molecular machines, Rep. Prog. Phys. **75**, 126001 (2012).

[28] M. Doi, Second quantization representation for classical many-particle system, J. Phys. A **9**, 1465 (1976).

[29] M. Doi, Stochastic theory of diffusion-controlled reaction, J. Phys. A **9**, 1479 (1976).

[30] L. Peliti, Path-integral approach to birth-death processes on a lattice, J. Phys. (Paris) **46**, 1469 (1985).

[31] L. Peliti, Renormalization of fluctuation effects in $a + a \to a$ reaction, J. Phys. A **19**, L365 (1986).

[32] E. Smith and S. Krishnamurthy (unpublished).

[33] J. C. Baez and B. Fong, Quantum techniques for studying equilibrium in reaction networks, J. Complex Networks **3**, 22 (2014).

[34] S. Krishnamurthy and E. Smith, J. Phys. A: Math. Theor. **50**, 425002 (2017).

[35] N. G. van Kampen, *Stochastic Processes in Physics and Chemistry*, 3rd ed. (Elsevier, Amsterdam, 2007).

[36] E. Smith, S. Krishnamurthy, W. Fontana, and D. C. Krakauer, Non-equilibrium phase transitions in biomolecular signal transduction, Phys. Rev. E **84**, 051917 (2011).

[37] E. Smith, Large-deviation principles, stochastic effective actions, path entropies, and the structure and meaning of thermodynamic descriptions, Rep. Prog. Phys. **74**, 046601 (2011).

[38] E. Smith and S. Krishnamurthy, *Symmetry and Collective Fluctuations in Evolutionary Games* (IOP, Bristol, 2015).

[39] D. C. Mattis and M. Lawrence Glasser, The uses of quantum field theory in diffusion-limited reactions, Rev. Mod. Phys **70**, 979 (1998).

[40] J. Cardy, Field theory and non-equilibrium statistical mechanics, lecture notes, 1999, available at http://www-thphys.physics.ox.ac.uk/people/JohnCardy/notes.ps.

[41] F. Schlögl, On thermodynamics near a steady state, Z. Phys. **248**, 446 (1971).

[42] D. F. Anderson, G. Craciun, M. Gopalkrishnan, and C. Wiuf, Lyapunov functions, stationary distributions, and non-

equilibrium potential for reaction networks, Bull. Math. Biol. **77**, 1744 (2015).

[43] J. L. Cardy, Electron localisation in disordered systems and classical solutions in Ginzburg-Landau field theory, J. Phys. C **11**, L321 (1987).

[44] S. Coleman, *Aspects of Symmetry* (Cambridge University Press, New York, 1985).

[45] E. Smith and H. J. Morowitz, *The Origin and Nature of Life on Earth: The Emergence of the Fourth Geosphere* (Cambridge University Press, London, 2016).

[46] L. Sjögren, Lecture notes on stochastic processes, http://physics.gu.se/∼frtbm/joomla/media/mydocs/LennartSjogren/kap8.pdf and http://physics.gu.se/∼frtbm/joomla/index.php?option=com_content&view=article&id=110&Itemid=290.

[47] S. Krishnamurthy, E. Smith, D. C. Krakauer, and W. Fontana, The stochastic behavior of a molecular switching circuit with feedback, Biol. Direct **2**, 13 (2007).

[48] D. Schnoerr, G. Sanguinetti, and R. Grima, Comparison of different moment-closure approximations for stochastic chemical kinetics, J. Chem. Phys. **143**, 185101 (2015).